ADVANCED MATERIALS
www.advmat.de

Chirality-Induced Spin Selectivity: An Enabling Technology for Quantum Applications

Alessandro Chiesa, Alberto Privitera, Emilio Macaluso, Matteo Mannini, Robert Bittl, Ron Naaman,* Michael R. Wasielewski,* Roberta Sessoli,* and Stefano Carretta**

Molecular spins are promising building blocks of future quantum technologies thanks to the unparalleled flexibility provided by chemistry, which allows the design of complex structures targeted for specific applications. However, their weak interaction with external stimuli makes it difficult to access their state at the single-molecule level, a fundamental tool for their use, for example, in quantum computing and sensing. Here, an innovative solution exploiting the interplay between chirality and magnetism using the chirality-induced spin selectivity effect on electron transfer processes is foreseen. It is envisioned to use a spin-to-charge conversion mechanism that can be realized by connecting a molecular spin qubit to a dyad where an electron donor and an electron acceptor are linked by a chiral bridge. By numerical simulations based on realistic parameters, it is shown that the chirality-induced spin selectivity effect could enable initialization, manipulation, and single-spin readout of molecular qubits and qudits even at relatively high temperatures.

1. Introduction

The total electronic spin of a molecule (hereafter molecular spin) is a prototypical quantum object of great relevance for quantum technologies,[1–5] especially to exploit the unparalleled degree of control and flexibility offered by chemistry. Molecules present many appealing features, as outlined in **Table 1**. Molecular spin qubits can show long, temperature-resilient and engineerable coherence times.[6–16] They are easy to control by microwave or radio-frequency pulses,[13,17–19] which allows implementing one- and also two-qubit gates[20] if pairs of spin qubits are linked together.[21–23] Moreover, they can be assembled into very complex supramolecular structures with tailored interactions. This enables the chemical engineering of their magnetic properties[22,24–27] for specific quantum algorithms, as demonstrated for the Grover's algorithm implemented on the nuclear spin of a single $TbPc_2$ molecule.[28,29]

Most importantly, they can display many accessible levels providing multilevel elementary units (qudit) that increase the power of quantum logic[45–47] and support quantum error correction embedded within single molecules.[32–34,48,49] The ingenious design of the electronic structure has also enabled a promising step toward optical initialization and readout of molecular spin qubits with interesting

A. Chiesa, E. Macaluso, S. Carretta
Università di Parma, Dipartimento di Scienze Matematiche Fisiche e Informatiche
I-43124 Parma, Italy
E-mail: stefano.carretta@unipr.it

A. Chiesa, E. Macaluso, S. Carretta
INFN-Sezione di Milano-Bicocca
gruppo collegato di Parma
43124 Parma, Italy

A. Chiesa, A. Privitera, E. Macaluso, M. Mannini, R. Sessoli, S. Carretta
Consorzio Interuniversitario Nazionale per la Scienza e Tecnologia dei Materiali (INSTM)
I-50121 Firenze, Italy

A. Privitera
Department of Industrial Engineering (DIEF)
University of Florence
I-50139 Firenze, Italy

A. Privitera, M. Mannini, R. Sessoli
Department of Chemistry "U. Schiff" (DICUS)
University of Florence
I-50019 Sesto Fiorentino, Italy
E-mail: roberta.sessoli@unifi.it

R. Bittl
Freie Universität Berlin
Fachbereich Physik, Berlin Joint EPR Lab
D-14195 Berlin, Germany
E-mail: robert.bittl@fu-berlin.de

R. Naaman
Department of Chemical and Biological Physics
Weizmann Institute of Science
Rehovot 76100, Israel
E-mail: ron.naaman@weizmann.ac.il

M. R. Wasielewski
Department of Chemistry and Institute for Sustainability and Energy at Northwestern
Northwestern University
Evanston, IL 60208-3113, USA
E-mail: m-wasielewski@northwestern.edu

The ORCID identification number(s) for the author(s) of this article can be found under https://doi.org/10.1002/adma.202300472

DOI: 10.1002/adma.202300472

Table 1. Potential of molecular spin qubits.

i) Long T_1 and T_2 (at room T)	ii) Quantum gates	iii) Chemical engineering of the Hamiltonian
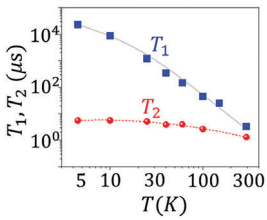 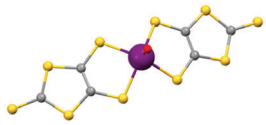	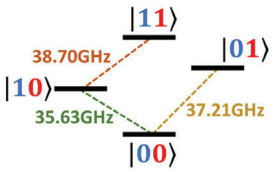 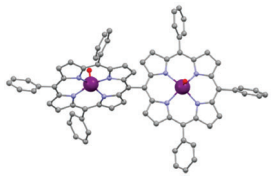	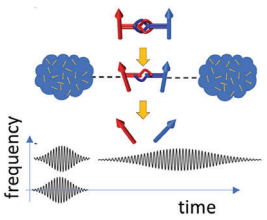 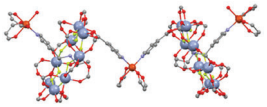
[7,8,13,30]	[20–23]	[27,31]
iv) Quantum algorithms	**v) Embedded quantum error correction**	**vi) Processability and hybrid structures**
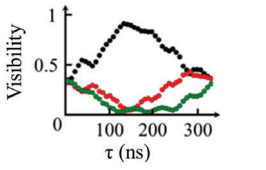 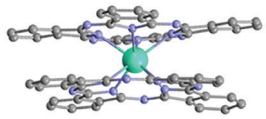	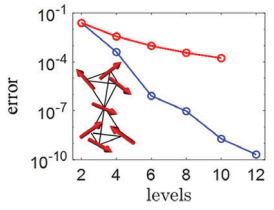 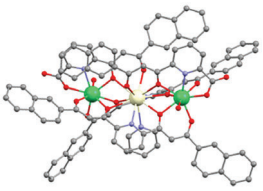	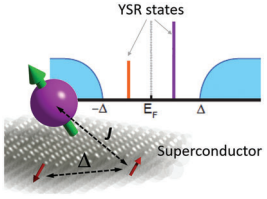 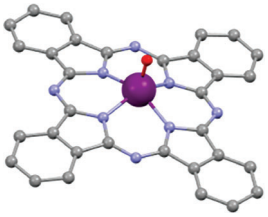
[28]	[17,32–34]	[35–44]

Each column refers to a different achievement/capability. In the different rows, we report the experimental results/schemes, the related molecular structures, and the relevant references. i) Very long coherence times stable up to room temperature,[13,30] close to ms for V^{4+} complexes with nuclear spin free ligands,[8] and tunable with suitable experimental conditions, such as the magnetic field close to atomic-clock transitions.[7] (Top figure in (i): adapted with permission.[13] Copyright 2016, American Chemical Society). ii) The possibility to link qubits together to implement entangling quantum gates,[21–23] for example, by pulse electron paramagnetic resonance techniques.[20] iii) The capability to chemically engineer the spin Hamiltonian to meet requirements for the implementation of specific algorithms[27,31] (Top figure in (iii): adapted with permission.[27] Copyright 2022, American Chemical Society). iv) Implementation of quantum algorithms (such as Grover's) on molecular spin qudits.[28] (Top figure in (iv): reproduced with permission.[28] Copyright 2017, American Physical Society). v) Potential of molecular spins to provide many accessible levels which can be exploited to embed quantum error-correction[17,32,33] suppressing pure-dephasing by orders of magnitude.[34] (Top figure in (v): adapted with permission.[34] Copyright 2022, American Chemical Society). vi) Processability into hybrid structures and organization onto metallic and superconducting surfaces,[35–40] tuning their coupling with the substrate, while keeping their magnetic properties and enabling manipulation of electronic[41] and nuclear spins.[42] Color code for molecular structures: C gray; N pale blue, O red, S yellow, V purple, Cu orange, Ni and Cr blue, Tb cyan, lanthanides in (v) green and white.

perspectives for integration in quantum networks.[50,51] Finally, molecular spins can be processed into hybrid structures and organized on surfaces[35–40,43] or within superconducting resonators.[41,42,44]

In this context, spin-correlated radical pairs (RPs) generated by photoinduced electron transfer (PET) have also been proposed for quantum information, because of their natural existence in entangled Bell states and the possibility of achieving atomic-scale control and interaction with other degrees of freedom, such as photons, charges and phonons.[52] However, the weak interaction of molecular spins with external magnetic (or electric) fields may limit some applications in quantum technologies to low temperatures and constitutes a potential limitation for the read-out of the spin state in single molecules.

We envision here an original solution for this problem in the combination of spin and chirality through the still relatively unexplored chirality-induced spin selectivity (CISS) effect.[53–57] The phenomenon was first observed in transport measurements: if an electron subject to an electric bias travels through a chiral medium, transmission is favored for a certain projection of

the spin of the electron along the chiral axis and suppressed for the other. Which orientation is preferred depends on the chirality handedness and on the direction of electron's motion. Remarkably, no magnetic field is required and CISS is very effective even at room temperature. Further experimental pieces of evidence have emerged in very different setups with no steady-state current[58–61] and even in PET through a chiral bridge.[62] However, these numerous experimental demonstrations have not yet converged into a unified theoretical description of the phenomenon,[63] although important advances have recently been made.[64–66] To make substantial progress in this direction, we should start from the observation of CISS in PET[62] and significantly simplify the experimental setup. In particular, one should remove all inessential ingredients such as metal leads, magnets, and other complex interfaces and focus on a chiral bridge linking an electron donor and an electron acceptor. Targeted magnetic resonance experiments can then be designed to assess the state of the spin wavefunction after PET[67–70] and hence unravel the nature of CISS. This will be the starting point to bring CISS and its potential applications to the single-molecule level. Because of CISS, PET will then result in a locally spin-polarized charge-separated state after the electron has crossed the chiral linker.

By adding a molecular spin qubit to the electron donor/acceptor pair it will be possible to transform CISS in a quantum-enabling technology. As proposed in this perspective, CISS has the potential to transduce the spin information into charge information because the electron is preferentially transmitted if it has the right spin orientation. Since the charge is much easier to read, this allows us to conceive a setup for single-molecule initialization and readout. Moreover, this spin selection and transduction should also work at room temperature.

In the following, we first provide a brief overview of the most important achievements in the use of photoinduced spin-correlated RPs for quantum technologies. Next, we summarize the main experimental demonstrations of CISS and recent efforts toward its quantum detection at the molecular level, which represents the starting point for applications in quantum technologies. We then show by numerical simulations that high-temperature initialization, readout of individual molecular qubits, and one- and two-qubit gates could be achieved on the proposed architecture. We include the most important sources of errors (such as charge-recombination, dephasing, and relaxation), finding very promising results in the aforementioned quantum information processing steps. We then discuss the chemical tools and challenges to actually implement the proposed architectures.

2. Electron Transfer for Quantum Technologies

Electron spins are good qubits because their two spin states constitute the quintessential two-level quantum system and they often display sizable coherence times. In addition, coupling two or more spins via the spin–spin exchange (J) and/or dipolar (D) interactions results in rich spin physics that allows generating quantum entanglement and implementing fundamental two-qubit operations. Based on the DiVincenzo criteria,[71] a critical requirement for a physical qubit is the preparation of a pure initial state. In addition, the preparation of two-qubit entangled states is necessary to execute fundamental quantum operations. These goals are difficult to achieve using the Boltzmann populations of the electron spin states because the energy gap between the states is small. For example, achieving >95% spin polarization requires millikelvin temperatures. In addition, if one uses the Zeeman interaction to increase the energy gap, even magnetic field strengths of about 10 T still require temperatures on the order of 4 K.

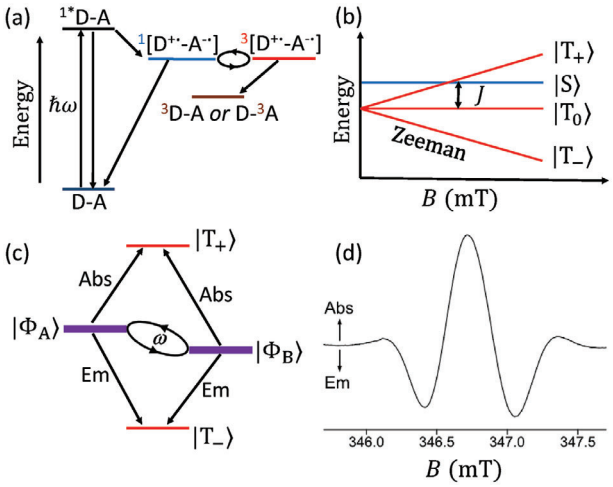

Figure 1. Scheme of the ET process. a) Energy level diagram for the states involved in PET after photoexcitation of the donor D in a donor–bridge–acceptor system. ^{1}*D–A denotes the excited singlet state of D, ^{1}[D$^{+\cdot}$–A$^{-\cdot}$] is the initial singlet pair state after PET, which coherently mixes with the ^{3}[D$^{+\cdot}$–A$^{-\cdot}$] triplet pair state, and ^{3}D–A, D–^{3}A are the molecular triplet states of D, A, respectively after electron recombination. b) Sketch of the Zeeman splitting of the four RP states resulting from the exchange interaction (J) between the two photogenerated spins. c) Sketch of the RP eigenstates at a specific magnetic field strength depicting the two unpopulated $|T_{+1}\rangle$ (red) and $|T_{-1}\rangle$ states and the two states $|\Phi_A\rangle$ and $|\Phi_A\rangle$ (purple), which are linear combinations of $|T_0\rangle$ and $|S\rangle$. They are populated according to their singlet character $|\langle S|\Phi_{A,B}\rangle|^2$. The singlet–triplet mixing due to Larmor frequency difference ω on D an A is indicated. d) trEPR spectrum with emissive (Em) and enhanced absorptive (Abs) features of the photoinduced RP state $P^{+\cdot}_{865}Q^{-\cdot}_{A}$ in photosynthetic reaction centers from *Rhodobacter sphaeroides*. Data taken from ref. [81] where experimental details are given.

Photoexcitation of an electron donor molecule (D) (**Figure 1**a) or an electron acceptor molecule (A) results in rapid charge separation to create a D$^{+\cdot}$A$^{-\cdot}$ RP provided the charge transfer step has a negative free energy and the coupling between the two moieties is sufficiently strong, a process well described by electron transfer theory.[72–76] In the absence of chiral media, fast electron transfer is considered to be spin conserving and the RP state inherits the spin state of the precursor molecular excited state, typically the excited singlet state of Figure 1a. This yields a population of the eigenstates of the RP far from Boltzmann equilibrium. Therefore, these states are referred to as spin-polarized RP states.[77–80] At high magnetic field, two of the RP eigenstates are pure triplet states ($|T_+\rangle$, $|T_-\rangle$, Figure 1b,c) and remain unpopulated in the case of a singlet precursor. Conversely, due to the different magnetic environments (Zeeman and hyperfine interactions) in D and A, the two remaining eigenstates $|\Phi_{A,B}\rangle$ are in general linear combinations of the third triplet state ($|T_0\rangle$) and the singlet state ($|S\rangle$) and are populated according to their singlet character $|\langle S|\Phi_{A,B}\rangle|^2$ (Figure 1c).

While optical spectroscopies are instrumental to characterize the kinetics and yields of PET down to the femtosecond time domain, they are typically insensitive to the spin properties of the RP state discussed above.[82–85] This information can advantageously be provided by time-resolved electron paramagnetic resonance spectroscopy (EPR) techniques, transient EPR (trEPR) and pulsed EPR. The spin states of PET-induced RP show rather peculiar properties in both time-resolved EPR techniques.[86,87] In addition, optically detected magnetic resonance (ODMR) can provide the sensitivity advantages of optical detection along with the ability to probe spin properties.[88]

The trEPR approach[89] uses continuous microwave (cw) irradiation, omits the magnetic field modulation/lock-in detection necessary in conventional cwEPR for sensitivity reasons, and gains time resolution by exploiting a light flash <10 ns and a broad bandwidth EPR resonator. Thus, trEPR is closely related to flash-induced absorbance spectroscopy with the continuous probe light replaced by microwave radiation for probing magnetic instead of electric dipole transitions. Experiments are performed by recording the transient response of the light-induced out-of-equilibrium state, for example, ^{3}D/^{3}A triplet states or RPs, at a fixed external magnetic field and successively stepping the magnetic field through the spectral width of the species of interest (for a review see, e.g., ref. [90]). The technique allows for a time resolution of ≈10 ns and is thus excellently suited to report the spin state of RPs.

Pulsed EPR on such systems adds the exciting light pulse and an additional variable time delay as elements to the repertoire of pulse sequences. The unique singlet-born RP population with its net zero integral EPR intensity results, for example, in a phase shift of the spin echo signal with a characteristic intensity modulation (out-of-phase electron spin echo envelope modulation, OOP-ESEEM) in which is encoded the spin–spin coupling of the RP.[87,91,92]

The non-Boltzmann population of spin states of the photoinduced RP results in highly characteristic features of enhanced absorption (Abs) and emission (Em) signals in trEPR (Figure 1d) with a net zero integral intensity over the whole spectral range. The initial spin state after the ET process also contains coherences between the eigenstates such that an overall singlet state (total spin $S = 0$) is preserved. As discussed above, this pure singlet state is in general not an eigenstate of the RP due to the different magnetic environments in D and A. Consequently, the overall spin state oscillates between singlet (S) and triplet (T_0) (Figure 1a,c). This phenomenon of coherent singlet–triplet oscillations has been predicted to be observable by trEPR on RP states in photosynthetic reaction centers.[86,93] It has been experimentally shown for the RP states consisting of the oxidized primary donor and the reduced (primary) quinone acceptor in photosystem I ($P_{700}^{+\cdot}A_1^{-\cdot}$)[94] and in a bacterial reaction center ($P_{865}^{+\cdot}Q_A^{-\cdot}$)[81] at ambient and cryogenic temperatures, respectively, and later also on a molecular triad.[95]

Recently, it has been shown that photogenerated RPs can be used for spin state teleportation in molecular triads consisting of a DA pair and an attached stable radical as a qubit (Q).[96–98] Photoexcitation of D results initially in the state $D^{+\cdot}A^{-\cdot}Q^{\cdot}$, with $D^{+\cdot}A^{-\cdot}$ generated in an entangled singlet $|S\rangle$, while $Q^{\cdot}$ is placed in an arbitrary spin state $|\psi\rangle$ using a microwave pulse before the photoexcitation (**Figure 2**a). The spontaneous ultrafast ET reaction $D^{+\cdot}A^{-\cdot}Q^{\cdot} \rightarrow D^{+\cdot}AQ^{-}$ constitutes a Bell state measurement

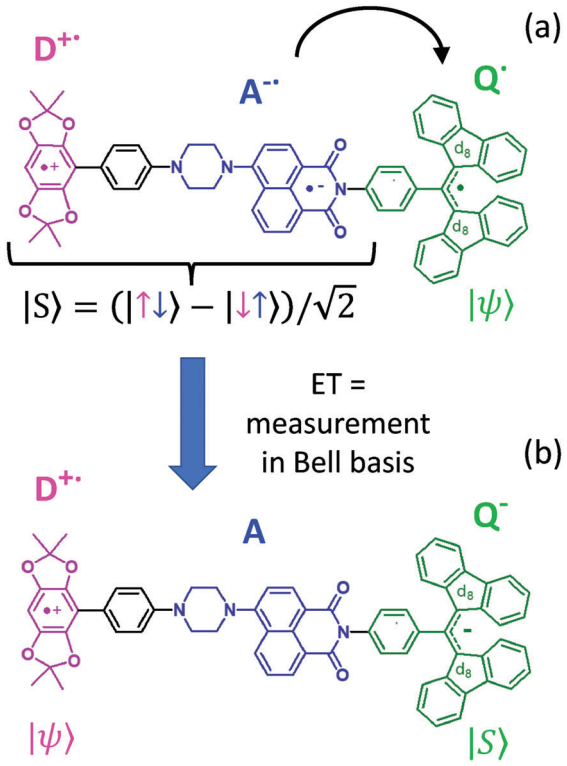

Figure 2. a) Quantum teleportation of the spin state $|\psi\rangle$ of radical $Q^{\cdot}$ to $D^{+\cdot}$ by exploiting the initial singlet pair shared by D and A (generated by a previous ET, not shown) and the subsequent ET from $A^{-\cdot}$ to $Q^{\cdot}$, which acts as a quantum measurement in the Bell (singlet–triplet AQ) basis. b) By selecting the $|S\rangle$ product state on Q^{-}, the former state of $Q^{\cdot}$ is teleported to $D^{+\cdot}$.

on AQ, as reported in Figure 2b. In the case of fast recombination of the triplet subensemble,[97] the final spin state of $D^{+\cdot}$ is the same $|\psi\rangle$ of $Q^{\cdot}$ before the electron transfer steps (Figure 2), thus achieving quantum state teleportation. Quantum state tomography of the initial $Q^{\cdot}$ and final $D^{+\cdot}$ spin states using pulse-EPR spectroscopy shows that the spin state of $Q^{\cdot}$ is indeed teleported to $D^{+\cdot}$ with high fidelity.[97] Extensions of this strategy may be able to transfer a spin state coherently across the 10–1000 nm distances that are important for quantum interconnects. Furthermore, a photoexcited RP can polarize a third spin,[99–102] and serve to implement a CNOT gate.[103] In addition, using *g*-factor engineering, individual spin qubit addressability can be achieved within a RP system.[104–106]

Concluding this section, we stress that the spin polarization induced by spin state preserving ET in achiral media is a two-spin property—leading to non-Boltzmann population of the four spin states of the pair—but does not correspond to a single-spin polarization. Conversely, the action of CISS on transmitted electrons provides this single-spin polarization and opens a variety of promising possibilities for quantum technologies, as discussed in the next sections.

3. Chirality-Induced Spin Selectivity

The CISS effect is a process in which the motion of an electron within a chiral potential is spin selective.[107] The effect exists also when the charge is reorganized within a chiral material, as a

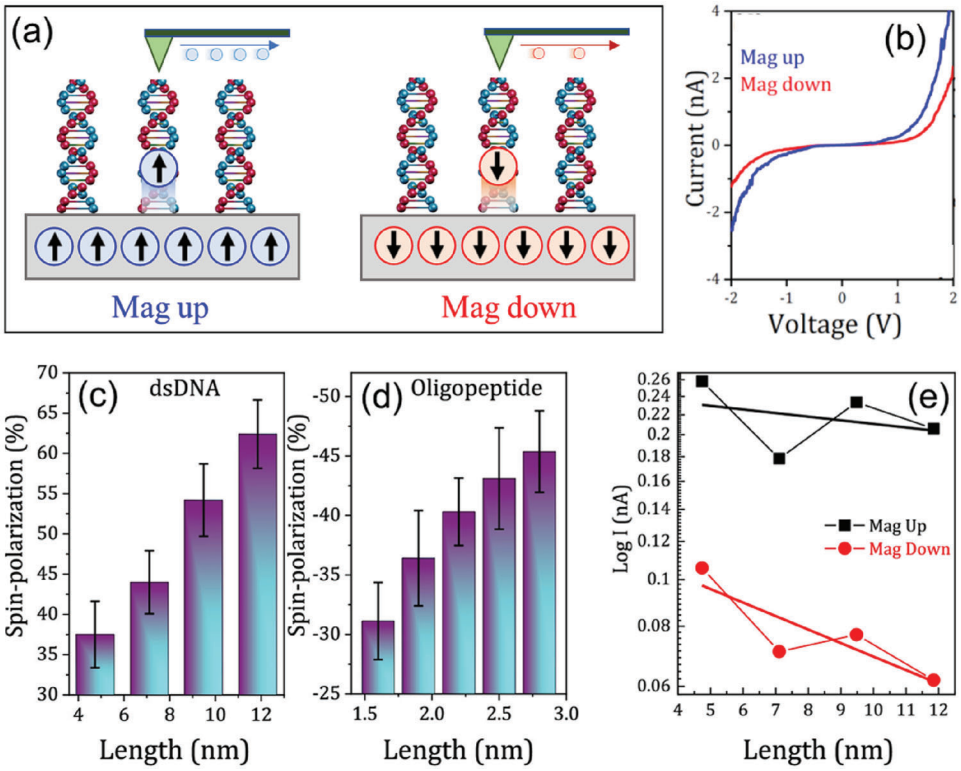

Figure 3. a) Schematic of the mc-AFM set-up used to detect CISS. The ferromagnetic substrate injecting spin-polarized electrons in the monolayer of chiral molecules is magnetized up or down with an external magnet. b) The average current versus voltage (IV) curves obtained for oligomers of dsDNA for up (I_u, blue) or down (I_d, red) magnetization of the magnet. c,d) Histogram summary of spin polarization, $P = [(I_u - I_d)/(I_u + I_d)] \times 100$ for various lengths of c) dsDNA and d) oligopeptide all measured at 2 V. e) Length dependence of the current measured for ds-DNA. The data shown are for a bias voltage of 1 V, when the substrate magnetization points up (black squares) or down (red circles). The slopes of the linear fits are in a ratio of three to one. Namely, the damping factor for transporting the unfavored spin decays three times faster than that of the favored spin. b–e) Reproduced with permission.[108] Copyright 2020, American Chemical Society.

result of applying an external electric field or of the interaction between the chiral object and another object.

Figure 3 presents the results of spin selective transport obtained with magnetic conducting atomic force microscopy (mc-AFM).[54,108] The substrate was a thin Ni film on top of which a few nm thick gold film layer was deposited. Figure 3b presents an example of experimental *I* versus *V* curves. Two phenomena can be recognized: first, the curves clearly show a nonlinear dependence of the current on the voltage, and second, the currents increase differently depending if the Ni film is magnetized up or down.[107,109] Figures 3c,d present the histogram summary of spin polarization for various lengths of double-stranded (ds) DNA and oligopeptides, respectively. Whereas the polarization measured for the two types of molecules is very similar, the polarization per unit length is about four times larger for the oligopeptides versus the dsDNA. The length dependence of the current measured for dsDNA is shown in Figure 3e. The slopes of the linear fits are in a ratio of three to one. Namely, the damping factor for transporting the unfavored spin decays three times faster than that of the favored spin. The observed behavior points to: i) A different barrier for injecting electrons with opposite spins into the chiral molecules; ii) The spins do not flip within the molecules, since such flipping would manifest into the same injection voltage for the two measured spins; iii) The coupling of the linear momentum of the electron with its spin enhances conduction by protecting from back scattering.

Remarkably, very high spin polarization at room temperature was observed in various systems, for example, up to about 90% in supramolecular wires.[110] Similar values were obtained for 2D chiral hybrid lead-iodide perovskites[111] and in chiral hybrid copper halides.[112] Close to 100% spin polarization was also observed in metal–organic frameworks (MOF).[113] The phenomenon of spin selectivity was observed also for single molecules using break junctions with scanning tunneling microscopy (STM)[61] or by measuring a single helicene molecule by AFM[114] However, neighboring molecules can also play a key role. A recent study showed that the organization of a monolayer affects the magnitude of the spin polarization.[115]

There is an extensive debate on the role of spin–orbit coupling on the leads in inducing the CISS effect.[19,116] In photoemission, the CISS effect was shown to depend only weakly on the spin–orbit coupling of the substrate,[117] but recent results may suggest a strong dependence on the substrate properties.[118] This exemplifies the importance of simplifying the setup in order to gain a deeper understanding of the origin of CISS.

When a chiral system is in its singlet state, namely all electrons are paired, and an electric field is applied, charge

polarization occurs and it is accompanied by transient spin polarization.[119] It is important to appreciate that since the electron density displaced in the chiral medium has a preferred spin, this motion breaks the entanglement. The extent of disentanglement in the singlet system depends on the amount of electron density that is displaced. The same argument holds for photoexcitation of chiral system that results in electron transfer. Also in this case, the entanglement of the electrons in the initial singlet state is broken. An interesting case is the study on the photosystem I, where it was shown[62] that photoexcitation of the chiral system results in spin-selective transport.[94,120,121] Additional strong evidence of spin selectivity for electron transfer through chiral molecules is the tenfold difference in electron-transfer rates between quantum dots (QDs) in chiral QD assemblies upon excitation with opposite circular polarization of the light.[122]

Although the spin polarization that accompanies charge polarization is a transient effect, the polarization can be stabilized by interaction with a ferromagnetic substrate or with another chiral system. It is important to appreciate that the interaction of two objects always involves charge reorganization due to their different electrochemical potentials and dispersive forces, for example, induced-dipole–induced-dipole interaction. Hence, if the two systems that interact are chiral, they become spin polarized during the collision and the spin-exchange energy can either stabilize or destabilize the combined system.[123] If the chiral system interacts with a ferromagnetic substrate, the transiently polarized spins in the chiral system may interact with the ferromagnet's spins by spin exchange. This interaction is responsible for enantiospecific interaction of chiral molecules with ferromagnets[60] and for enantioselective crystallization on those surfaces.[124] The spin-exchange interaction can even realign the spin in the ferromagnetic domains, and the binding of the chiral system to the surface will result in stabilizing the spin polarization in the system.[125]

To conclude this section, we note that one of the most peculiar features of CISS is the clear enhancement of the effect with increasing temperature, as shown in ref. [126]. This suggests the crucial role vibrations could play in explaining the phenomenon, as pointed out by Fransson[65,66,126] and by a recent work on the interplay between spin–orbit coupling and nuclear motion in ET.[127]

4. Quantum Detection of CISS

The investigation of CISS in PET processes has several advantages but has remained mostly unexplored. Indeed, CISS could be detected at the molecular level and not in complex heterostructures, thus focusing on the main player, that is, the chiral molecule. Moreover, the use of magnetic resonance would enable for the first time direct access to the electron state after CISS by performing a full tomography. This in turn would finally reveal the true nature of CISS and provide the missing information needed for a sound understanding of the phenomenon.

The first model of the CISS effect in PET reactions was proposed in ref. [67], based on the solution of the Nakajima–Zwanzig equation with coupling between the two charge transfer states including spin–orbit interaction. With these assumptions, the CISS effect translates into a rotation of the spin of the transferred electron giving rise to spin coherence and not to spin polarization. The latter can be detected by the OOP-ESEEM EPR experiment. Later on, an alternative mechanism was proposed, which dynamically produces spin polarization in incoherent PET through an intermediate state and is mediated by both spin–orbit and exchange interaction between spins of the RP.[128]

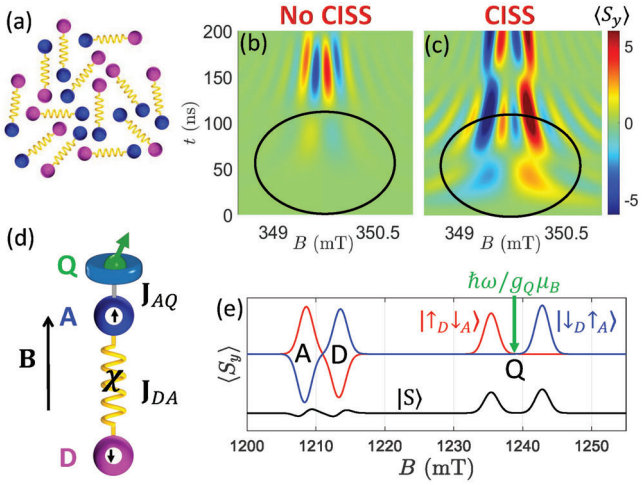

Figure 4. a–e) Quantum detection of CISS in PET by magnetic resonance in an isotropic solution of D–χ–A molecules (a–c) or using a qubit as a sensor of the transferred polarization in an oriented sample (d,e). Simulated time and magnetic field (B) dependence of the trEPR signal for different precursor states: b) a pure singlet, c) a polarized state originating from 100% CISS. d) Scheme of the donor (D), chiral bridge (χ), acceptor (A), qubit (Q) system proposed to detect spin polarization on A after ET. The magnetic field **B** is parallel to the χ axis and dipolar interactions between DA $\mathbf{J}_{DA}$ and AQ $\mathbf{J}_{AQ}$ are assumed. e) Integrated trEPR Q-band spectrum, showing the Q signal at higher field ($g_Q = 1.96$ as for VO) and that of DA ($g_{D,A} = g_e \mp 0.001$) at low field, with Q initially in $|\downarrow_Q\rangle$. In the absence of CISS, black line and singlet state for the D/A pair, the Q signal is split into two lines. CISS-induced full polarization results in the disappearance of one of the two qubit excitations, depending on the enantiomer (red and blue lines). Adapted with permission.[69] Copyright 2021, American Chemical Society.

As first proposed in ref. [68], polarization effects in PET could be detected on oriented samples of chiral molecules, either by comparing spectra recorded with the magnetic field parallel or perpendicular to the chiral axis or in the in-phase channel of an OOP-ESEEM measurement. Moreover, the model proposed in ref. [68] for CISS in forward and backward ET reactions breaks time-reversal symmetry and leads to a dependence of the recombination yield on the magnetic field orientation.

A significant simplification of the setup was proposed in ref. [69]. Indeed, it was shown that one can unveil the occurrence of CISS in the short-time trEPR spectrum even of a randomly oriented solution (**Figure 4**a) of donor–(chiral bridge)–acceptor units (D–χ–A hereafter), in presence of an anisotropic (e.g., dipolar) spin–spin donor–acceptor interaction . The different initial populations between the isotropic singlet ($|S\rangle$) and the highly anisotropic polarized state $|\uparrow\downarrow\rangle$ expected for CISS give rise to an opposite order in the absorption/emission peaks (Figure 4b,c). Indeed, 2 CISS filtering gives rise to a different population of the eigenstates depending on the orientation of the chiral axis χ with respect to the magnetic field **B**, and in particular to a

prevalence of the population of T_+ and T_- compared to T_0 for $\chi \perp \mathbf{B}$. This eventually yields an opposite Abs/Em pattern compared to the singlet precursor in the spherical average.

A deeper insight into the state of the RP wavefunction after ET through a chiral linker can be gained[69] by considering an ordered system of D–χ–A molecules in a magnetic field parallel to the χ axis and with a molecular spin qubit (Q) linked to the acceptor, as sketched in Figure 4d. The latter acts as a coherent sensor of the polarization of the RP after PET. Hereafter we focus on this setup, which constitutes the elementary building-block of the quantum computing architecture proposed below.

To simplify the discussion we assume from now on a singlet state precursor with negligible inter-system crossing. The trEPR signal $\langle S_y \rangle$ is shown in Figure 4e, for different possible states of the RP at the beginning of the measurement and with the qubit initially in $|\downarrow_Q\rangle$. The black line corresponds to the $|S\rangle$ state for the RP, while the red and blue traces indicate polarized spin states with opposite polarizations ($|\uparrow_D\downarrow_A\rangle$ and $|\downarrow_D\uparrow_A\rangle$), as expected from CISS acting as a spin filter.[67,68] By focusing on the qubit signal, at higher field in our simulation, one can clearly distinguish the three RP states. Indeed, if both acceptor spin states are populated, the peak corresponding to a bare excitation of the qubit (green arrow in Figure 4e) is split by the A–Q coupling. In the case of a completely non-polarized A state, the polarization $p = -2\mathrm{Tr}[\rho s_z^A] = 0$, thus the relative intensity of the two peaks is approximately the same. By varying p, their relative intensity changes, until one of them completely disappears in case of a completely polarizing ($p = \pm 1$) CISS effect. Changing the enantiomer changes the sign of p and hence swaps the relative intensity of the two peaks. Interesting information can also be gained from the DA signal at lower field in Figure 4e, where the four transitions occurring for the singlet (see Figure 1c) are reduced to only two intense peaks (one in absorption and the other in emission) for $p = \pm 1$. It is finally worth mentioning that equivalent knowledge could be obtained from broadband nuclear magnetic resonance (NMR) experiments,[69] where a nuclear spin hyperfine coupled to the acceptor electronic spin works as a probe of A polarization.

The same setup can also be exploited to transfer polarization from A to Q by a simple sequence of resonant microwave (mw) pulses, as described in the next section. The detection of trEPR spectrum after this process would provide another way to identify clear signatures of CISS, as described in ref. [69].

5. CISS-Mediated Initialization and Readout of Single Molecules

As already mentioned, CISS effect is still not well understood from a theoretical point of view,[63] although recent progress has been made.[65,66,126] Here we envisage how CISS could be exploited as an enabling technology for quantum applications, relying on general characteristics of the phenomenon. The latter is phenomenologically described as in refs. [68, 69], without referring to a specific microscopic model. In particular, we propose exploiting CISS to initialize, implement two-qubit gates and readout the state of individual molecular spins. Besides microwaves, we plan the use of an electric field as a manipulation tool to facilitate ET or induce recombination.

5.1. Initialization of Molecular Spins

The need for ultralow temperatures to faithfully initialize qubits is a major limitation of most current technologies for quantum computing. Conversely, operating qubits above He liquid temperatures would allow one to reduce the required cooling power by orders of magnitude.[129] Here we illustrate a method (in the line of ref. [69]) for transferring spin polarization from A to Q by a simple sequence of resonant microwave (mw) pulses, which works even at high temperatures. Indeed, as remarked above, both CISS-induced polarization[126] and coherence of molecular spin qubits (such as VO^{2+} or Cu^{2+} complexes) are very large even at room temperature.[13,30]

The two π pulses (I,II) needed for such a polarization transfer are schematically shown in **Figure 5**a, where thick lines represent the initial population of the AQ pair energy levels, while the inactive state of D is omitted for clarity. From now on, we use the quantum computing notation $|\downarrow\rangle \equiv |0\rangle$ and $|\uparrow\rangle \equiv |1\rangle$. We start from a fully polarized state of A after PET, while the two states of Q are (almost) equally populated. After pulses I and II in Figure 5a, Q is fully polarized and A is in a mixed state.[130]

The corresponding simulation is reported in the blue-shaded area of Figure 5b and demonstrates that high-fidelity initialization can be achieved even by assuming coherence (T_2) and relaxation times (T_1) typical of molecular spin qubits at room temperature. Indeed, starting with a perfectly polarized state with $\langle s_z^A \rangle = 1/2$ and $\langle s_z^Q \rangle = 0$, by applying a pair of resonant Gaussian pulses (sketched in the bottom part of the figure) with peak amplitude 30–50 G lasting about 20 ns, we get $\langle s_z^Q \rangle$ close to 1/2 (with an error below 1%). In the simulations we are considering a Cu^{2+} qubit, $g_Q = (2.1, 2.1, 2.3)$, in a magnetic field of 1.05 T, typical of Q-band EPR. This ensures well-factorized eigenstates for the three spins. The qubit is coupled to the acceptor through isotropic exchange $J_{AQ} = -0.02$ cm^{-1} (but dipole–dipole interaction would work as well) and with $T_2 = 0.6$ µs as reported in ref. [30] for a Cu^{2+} qubit at room temperature. Spin dephasing on D/A was included using reasonable values of 1 µs, as well as spin-selective charge recombination with rate 0.1 µs^{-1}.

Having initialized the state of the qubit, logical quantum operations can be implemented. For instance, we can employ pulses resonant with the qubit transitions (II and III in the right panel of Figure 5a) to implement single-qubit rotations $R_{x,y}(\vartheta)$ of arbitrary angles about x or y axis. In particular, we show in the yellow-shaded region of Figure 5b an $R_y(\pi)$ gate, bringing $\langle s_z^Q \rangle$ from 1/2 to −1/2. After qubit manipulations, quantum information can be swapped back to the acceptor spin by reversing the pulse sequence used for qubit initialization (right red-shaded area in Figure 5b). Results of this "back-swap" are shown for the two logical states of the qubit. This is the first step for reading out the qubit state by spin-to-charge conversion induced by spin-selective recombination[68] (see next subsection) and to initialize a multilevel molecular spin (qudit).

Qudits represent a crucial resource of molecular spins for quantum error correction and computing.[4] Hence, it is worth exploring a way to initialize also these multilevel systems. If we start from a polarized spin 1/2 acceptor as in the sequence of Figure 5a, we can only initialize another two-level system. In fact, at the end of the pulse sequence, A is in a mixed and not polarized state. The problem can be circumvented by using an

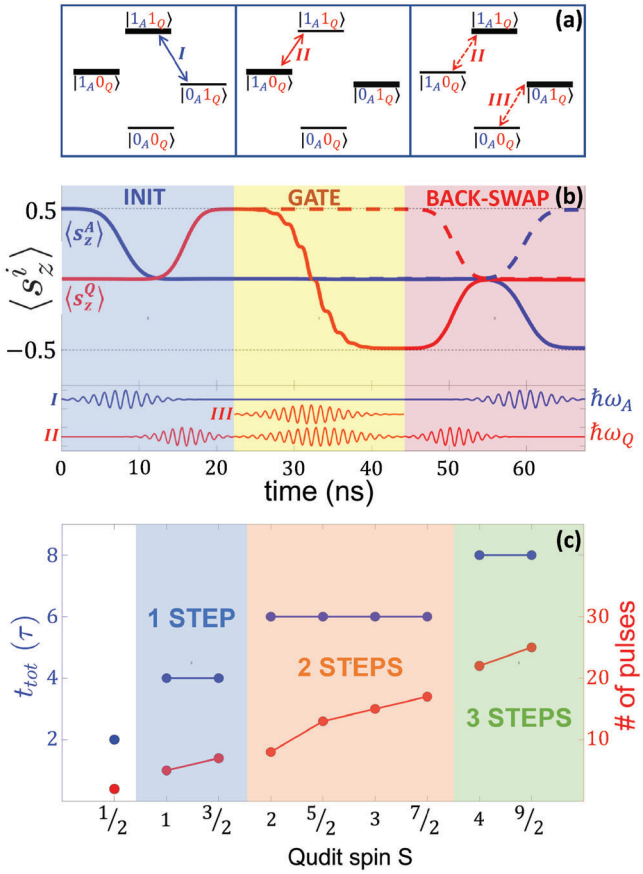

Figure 5. a) Sequence of pulses addressing specific transitions of the AQ spin pair (with $|\downarrow\rangle \equiv |0\rangle$ and $|\uparrow\rangle \equiv |1\rangle$), where the state of D has been omitted. Blue (red) colors refer to A(Q), while level thickness indicates the population of each level before the reported pulse. After pulses I and II for initialization, the states of $|10\rangle$ and $|01\rangle$ have been swapped and single-qubit gates can be implemented (dashed double-arrows in the last panel). b) Time evolution of the expectation value of the local spin s_z^j for j = A (blue) and j =Q, subject to the sequence of pulses (sketched below) needed to initialize Q (blue shaded area), to implement a single-qubit rotation on Q (corresponding to a spin flip, yellow shaded) and to swap back the logical state from Q to A (red-shaded region). The latter is reported for the two logical states of the qubit (solid vs dashed lines). c) Scaling of the estimated number of pulses and recombination-charge separation (RS) to fully polarize a molecular spin qudit S. The number of RS steps is indicated by different colors and the total duration of the scheme is displayed in units of the duration τ of a single mw π pulse (≈10 ns). Results are computed by assuming simultaneous mw pulses to address independent transitions and by neglecting the much smaller time required for RS steps.

external knob (such as an electric field or a laser pulse, see below) to induce charge recombination and, subsequently, another charge separation. By inducing this charge recombination–separation (RS) process through χ, the traveling electron is repolarized. Therefore, this tool can be exploited to initialize a spin qudit by a multistep procedure. To this end, we have designed a sequence of mw pulses and RS steps allowing to fully polarize a spin S system (with $2S+1$ levels) and we have investigated the scaling of required resources by increasing S. Remarkably, as shown in Figure 5c, both the number of RS steps and the overall duration of the initialization process show a slow increase with S. Given the fast ET (sub-nanosecond), the total time of the initialization practically coincides with the duration of the mw pulses (each lasting ≈10 ns), implemented in parallel for transitions between independent pairs of levels.

The scheme presented in Figure 5c requires the capability to drive charge recombination by an external manipulation tool. Two different routes can be envisaged for such a task: the first possibility is to use light to photoexcite the acceptor, thus providing the driving force for fast recombination.[85,131] The second one is to exploit an electric field to modulate electron transfer rates by changing the energy levels of donor and/or acceptor and hence the activation energy. In fact, in Marcus' theory this can lead to an exponential modulation of the electron transfer rates,[132,133] with a variation of several orders of magnitude in a reasonable electric field range. The latter can be turned on and off on ns timescale[134,135] by exploiting pulsed electric-field technology used for instance to study biological systems.[136] The same method can also be exploited to facilitate PET in case of rather long χ bridges that are typically employed to enhance spin selectivity. Besides qudit initialization, the possibility of inducing forward and backward ET at will also enables single-spin readout, as described below.

5.2. Readout by Spin-to-Charge Conversion

We now illustrate how to exploit spin-selective recombination due to the CISS effect to convert the spin into charge information. The scheme is based on the simple phenomenological model of CISS on reverse electron transfer proposed in ref. [68]. Such a mechanism would allow the readout of a single molecular spin in analogy to what is currently done in semiconductor qubits, but at significantly higher temperatures. Indeed, spin-to-charge conversion is the most established readout method for quantum dots (QDs) or impurity donors in semiconductors.[137] Two of the state-of-the-art techniques are reported in **Figure 6**a,b: the charge displacement between a semiconductor qubit (SC-Q) and either a reservoir (a) or a single-electron transistor (SET, yellow sphere (b)) is made spin dependent by electrically tuning the electrochemical potential of the reservoir or of the SET.

We focus on the first method, described in Figure 6a. In an applied magnetic field, the two states of a single spin 1/2 QD used to encode a qubit are split by the Zeeman interaction. Hence, also the respective chemical potentials $\mu_\uparrow$ and $\mu_\downarrow$ (representing the energy required to add an electron with either spin ↑ or ↓ to the QD) are different. Then, the electrochemical potential of a nearby electron reservoir μ_R is set such that $\mu_\downarrow < \mu_R < \mu_\uparrow$. In these conditions, if the QD is in state $|\downarrow\rangle$, tunneling out from the QD is prevented by Coulomb blockade because all the levels in the reservoir are filled at that energy. Only if the QD is in state $|\uparrow\rangle$ it will tunnel from the QD into empty states of the reservoir. The associated charge displacement (occurring only for one of the two qubit states) changes the electrostatic potential in its proximity and can therefore be recorded by a nearby electrometer, such as a quantum point contact,[140,141] another quantum dot[142] or a SET, as shown in Figure 6a. Usually, a peak in the current, for example, flowing through the SET as in Figure 6a, is measured as soon as the charge on the QD changes. The current returns to its original

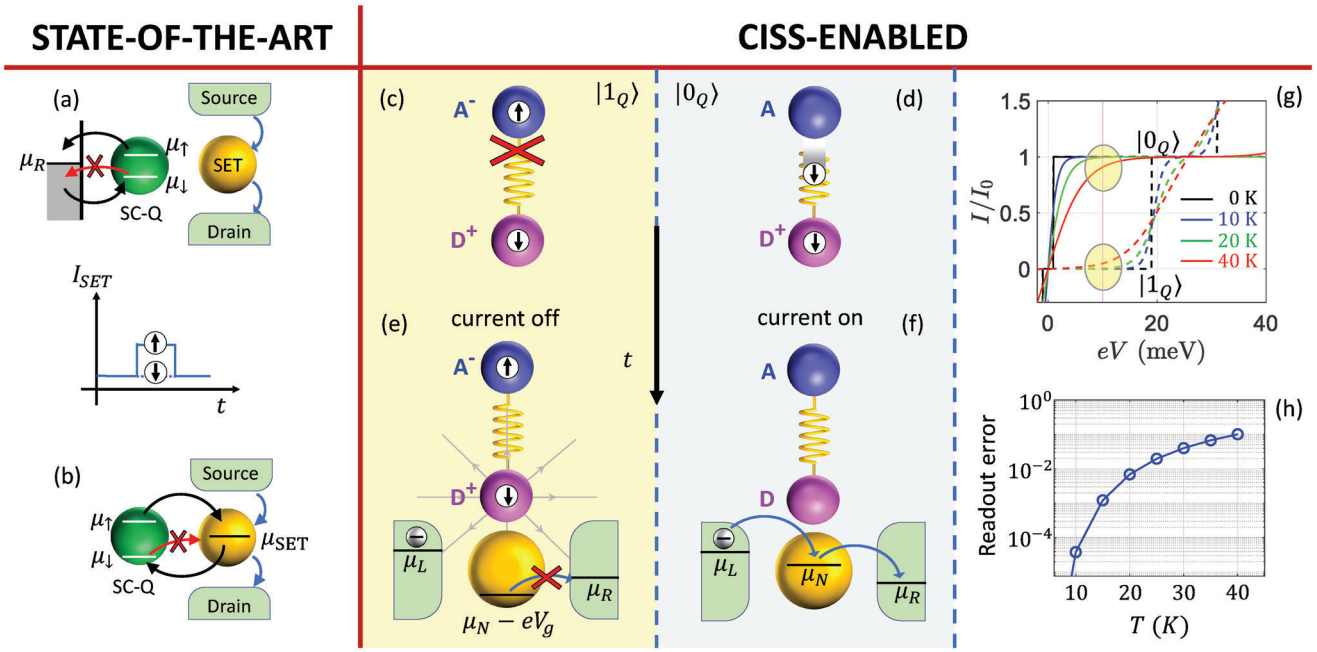

Figure 6. a,b) State-of-the-art methods for readout based on spin-to-charge conversion in quantum dots or dopants in semiconductors. Here the tunneling of the semiconductor qubit (SC-Q) either to a nearby reservoir (a) or to a SET (b) is made spin dependent by energy selection based on Zeeman splitting. In both cases, this yields a peak in the current flowing through the SET. c–f) CISS-based spin-charge locking and associated scheme to readout the state of a single molecular spin by measuring the current through the SET. The situations corresponding to the two possible states of the qubit ($\uparrow \equiv |1_Q\rangle$ and $\downarrow \equiv |0_Q\rangle$) are sketched in the yellow and gray shaded area, respectively, with time increasing from top to bottom. c) After swapping the qubit state to the acceptor, if the qubit is in $|1_Q\rangle$ it is blocked by CISS, d) while it is allowed to recombine only if it is in $|0_Q\rangle$. e) The charged radical pair generates an electric field which shifts the electrochemical potential of the dot μ_N, thus preventing the current to flow, f) while in the recombined DA state, the donor is neutral and current flows through the dot. g) Corresponding simulation of the current as a function of the bias voltage, for neutral (continuous lines) and charged (dashed) DA at different temperatures T. h) Readout error as a function of T, computed at the bias voltage indicated by the vertical line. In the simulations we assume a CdSe quantum dot with $\mu_N = (N - 1/2)U + \epsilon - eV_g$, where N is the excess number of electrons, U is the charging energy of the dot, ϵ the orbital level spacing, and V_g a gate voltage.[138] For a small-size CdSe dot of diameter ≈6 nm it is reasonable to set $U = 50$ meV, $\epsilon = 1$ meV[139] and a gate potential $eV_g = 20$ meV.

value as soon as a new electron tunneling from the reservoir to the QD reinitializes it into its $|\downarrow\rangle$ state.

Alternatively, a SET can act both as charge detector and reservoir, as usually done when qubits are shallow donors in semiconductors[143] and depicted in Figure 6b. Again, energy selection based on the Zeeman splitting is exploited to enable tunneling from the donor qubit (green sphere) to the SET only for one of the two qubit states ($|\uparrow\rangle$), a condition that activates a current through the SET. The current is then blocked again by a different electron tunneling back later onto the donor. Other spin-to-charge conversion methods exist (based for instance on Pauli exclusion principle on pairs of QDs instead of Zeeman-energy selection) for which we refer to more comprehensive reviews.[137]

Here we propose to exploit CISS to lock spin and charge, and then to readout the charge state of the donor by a sensitive electrometer similarly to Figure 6a. This CISS-mediated spin-charge locking does not rely on the small Zeeman energy scale[143] and therefore could work at much higher temperatures than those normally employed in semiconductor quantum dots or impurity spins.[144] In particular, let us consider a generic state of a D–χ–A–Q unit after having transferred the logical state of Q onto A, as shown in the red-shaded area of Figure 5b for the two possible logical states of Q (with either $\langle s_z^Q \rangle = 1/2$ or $-1/2$). We then induce charge recombination by electric field or light, as described above. Thanks to the CISS effect, such a recombination is spin selective and only occurs if the electron on A is in a specific spin state, as illustrated in Figure 6c,d. Following the simulations of Figure 5b (where the $|\uparrow\rangle \equiv |1\rangle$ state was favored in the charge separation process) here we consider selection of $|\downarrow\rangle \equiv |0\rangle$ state in the recombination.

After spin-selective recombination, the two different spin states of the qubit correspond to two different charge states of the DA dyad and can be distinguished by measuring the current through the SET. Indeed, the charge separation (CS) in $D^{+\cdot}A^{-\cdot}$ generates a gate voltage V_g on the SET, which is absent for the neutral DA after charge recombination. Such a gate voltage shifts the chemical potential μ_N of the SET, thus getting in and out of the bias window and hence turning on and off the current, as sketched in Figure 6e,f. For a fixed bias voltage, one can distinguish between "current off" (in the charged state, (e)) and "current on" (in the neutral state, (f)). By measuring the current, the former state of the qubit $|0_Q\rangle$ (current on) or $|1_Q\rangle$ (current off) is then measured.

An alternative, in the line of Figure 6b, is to use the donor as the SET in Figure 6e,f. This could be realized by using, for instance, a CdSe nanoparticle, already employed to generate RPs.[70,106] Then, one would measure a jump in the current when the charge on the SET changes as a result of the spin-dependent back transfer.

Simulations of the readout process are shown in Figure 6g, obtained by numerically computing the steady-state solution of the second-order Pauli master equation[145,146] for the two states of the qubit, assuming ideal CISS. The effect of temperature is included via the Fermi functions on the electrodes, while co-tunneling processes and the broadening of the SET levels, due to the coupling with the electrodes and finite level lifetime, are neglected. This approximation is acceptable if the charging energy is in the order of 50-60 meV range, as for CdSe nanoparticles.[139,147] At fixed bias voltage (vertical magenta line), we define the readout error reported in Figure 6h as $\mathcal{E} = 1 - [(I_0 - I_1)/(I_0 + I_1)]$. Clearly, $\mathcal{E} \to 0$ at $T = 0$ and increases with temperature, due to the smearing of the Fermi functions which is reflected in a smoothing of the current staircase. In order to minimize $\mathcal{E}$, one needs to make the gate voltage eV_g associated with the electric field generated by the RP as large as possible, and in particular much larger than $k_B T$. Here we are considering a SET consisting of a CdSe quantum dot of diameter 6 nm with D 1 nm apart from the surface and a DA distance of 2 nm. Using the dielectric constant reported for CdSe nanoparticles[148] $\epsilon/\epsilon_0 = 6$, one could estimate $eV_g \approx 20$ meV by assuming the dielectric filling the whole space. For a dielectric sphere surrounded by vacuum mimicking the SET, significantly higher values could be achieved,[149,150] which would further increase the operating temperature of the device. Nonetheless, here we prefer to make the conservative assumption $eV_g \approx 20$ meV to account for other possible charge screening effects and/or for a less favorable geometry in a practical realization, for example, with D farther from the SET. Remarkably, even by using these values, we find a readout error of only ≈0.01 at 25 K (Figure 6h).

Finally, a few comments on the hierarchy between different parameters are in order. We work in the sequential tunneling regime, which requires the SET-lead tunneling rate Γ to be smaller than $k_B T$.[151] In addition, the time-scale of the readout procedure $\tau_{RO} \approx 5\hbar/\Gamma$[143] must be significantly shorter than possible recombination from the singlet state, which is expected to occur after ET in case of imperfect CISS filtering. Nevertheless, the recombination rate k_0 from the polarized $|0_A\rangle$ state (as depicted in Figure 6d) will be much faster than that from the singlet, parameterized by k_S. This allows one to find a proper readout time $1/k_0 < \tau_{RO} < 1/k_S$, in which only the desired spin-polarized recombination has occurred. All of these constraints can be met by exploiting the flexibility of chemistry as discussed in Section 6 below.

5.3. Two-Qubit Gates

The proposed scheme can be extended to a multiqubit architecture. For instance, one could design a molecular system as sketched in the inset of **Figure 7**, with a pair of qubits Q_1 and Q_2 linked to the acceptor. This would allow one to exploit CISS also for implementing switchable two-qubit gates. In the idle configuration, A is neutral and the two qubits are practically decoupled, thus enabling the implementation of single-qubit operations. To switch on the two-qubit gate, an electron is transferred to A. Thanks to CISS, such an electron is in a well-defined spin state (such as $|\downarrow\rangle$) and its virtual excitations due to the interactions with $Q_{1,2}$ can be exploited to mediate an effective coupling

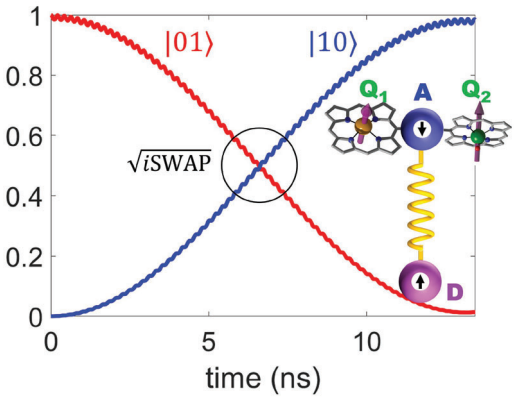

Figure 7. Simulation of an *i*SWAP gate between a pair of qubits Q_1 and Q_2, with an effective switchable interaction mediated by the acceptor spin (as sketched in the inset). The simulation is performed by assuming $B = 1.05$ T, two equivalent Cu qubits with $g_{1,2} = (2.1, 2.1, 2.3)$, coupled to the acceptor via an isotropic coupling $J = -0.02$ cm^{-1}. We also include the most important errors: spin dephasing on the qubits ($T_2 = 0.6$ µs) and on the RP ($T_{2,D} = T_{2,A} = 1$ µs) and spin-selective charge recombination with a rate of 0.1 µs^{-1}.

between the two qubits. The latter is kept on for suitable amount of time to implement an entangling gate and finally switched off again by inducing charge-recombination.

To assess the feasibility of the proposed scheme, we provide a more detailed derivation of the coupled two-qubit dynamics and of the hypothesis underlying our scheme. After CS, we consider a three-spin system described by the spin Hamiltonian

$$H = J(\mathbf{s}_1 \cdot \mathbf{s}_A + \mathbf{s}_A \cdot \mathbf{s}_2) + \sum_{i=1,A,2} g_i \mu_B B s_i^z \tag{1}$$

where $\mathbf{s}_1$, $\mathbf{s}_2$, $\mathbf{s}_A$ are spin 1/2 operators describing the qubits (1,2) and the acceptor (A), B is the applied field, g_i are the respective g factors, and J is the isotropic spin–spin coupling constant between each of the two qubits and the acceptor spin. We operate in a regime where $|g_{1,2} - g_A|\mu_B B \gg J$, which makes the eigenstates of the three-spin system practically factorized. This regime is easily reached using Cu-based qubits ($g \approx 2.3$) in a typical Q-band applied field (≈1 T), weakly coupled to A ($J \approx 10^{-2}$ cm^{-1}). Then, we focus on the subspace in which the acceptor spin is $|\downarrow\rangle$ (which is guaranteed by CISS) and we derive in such a subspace the effective Hamiltonian for the two qubits.[22,25] The latter takes the form

$$H_{eff} = \Lambda(s_1^x s_2^x + s_1^y s_2^y) + \lambda_1 s_1^z + \lambda_2 s_2^z \tag{2}$$

with

$$\Lambda = \sum_{i=1,2} \frac{J^2}{4\mu_B B(g_i - g_A)} \tag{3}$$

$$\lambda_i = g_i \mu_B B - \frac{J}{2} + \frac{J^2}{4\mu_B B(g_i - g_A)}$$

In practice, within the computational basis we obtain an effective XY interaction between the qubits, mediated by virtual excitations of the switch between its $|\downarrow\rangle$ and $|\uparrow\rangle$ states. Note that substituting

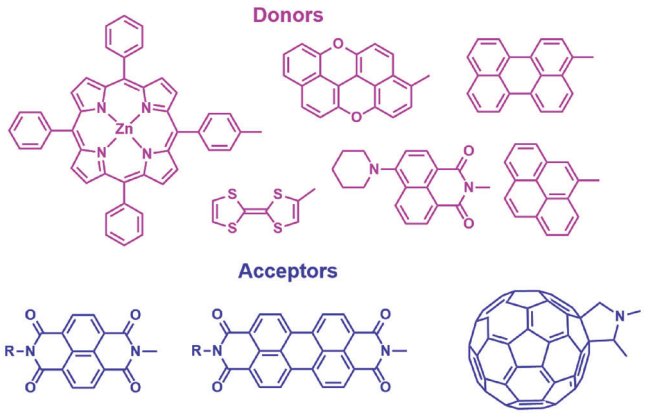

Figure 8. Selected electron donors and acceptors that have been incorporated into D–A dyads and triads that give long-lived CS states in an initial singlet spin state.

the isotropic interaction with a dipolar one would change the effective Hamiltonian but not the overall scheme.

If the two qubits have the same g_i the effective coupling acts to first order and implements an iSWAP$^{\alpha}$ two-qubit gate, when turned on for a suitable amount of time.[22,25,152,153] This is achieved by inducing ET and recombination by external stimuli, as described above, on a timescale much faster than $1/\Lambda$. The simulation of the time evolution of the qubit pair due to the Hamiltonian (1), yielding the effective coupling H_{eff}, is shown in Figure 7, with two identical Cu qubits characterized by the same parameters used in Section 5.1. The simulation shows that the two-qubit gate iSWAP$^{\alpha}$ is implemented in ≈10 ns with a fidelity exceeding 99%.

6. From Sketches to Real Systems

6.1. Challenges of the Chemical Design

The implementation of the control and readout schemes of previous sections relies on the identification of suitable D–χ–A dyads where the RP state lives long enough to allow the transfer of polarization to/from the qubit. Generally, the charge separation efficiency cannot be fully decomposed into individual contributions coming from the D/A and bridge building blocks.[154] Nevertheless, we will use this simplification to clarify our arguments.

6.1.1. The DA Pair

Several decades of investigations on intramolecular photoinduced ET have provided a wide library of molecules from which potential candidates for a quantum detection of CISS can be selected. The optimal energy level alignment of D's and A's frontier orbitals (HOMO and LUMO respectively) and the reorganization energy are the key ingredients to have a driving force for ET after excitation, as already shown in Figure 1. A selection of D/A molecules that have provided long-lived RPs is shown in **Figure 8**.

Also important is the spectral separation of the D and A excitations to allow discrimination in the photoexcitation, which is crucial for promoting selective oxidative or reductive PET. In oxidative PET, after donor excitation, a donor-to-bridge ET occurs and generates the $D^{+\cdot}$–$B^{-\cdot}$–A virtual (or real) state. In reductive PET, the electron is transferred from the bridge to the excited state of A, better visualized as a hole transfer (HT) from the excited A to the bridge, thereby generating the D–$B^{+\cdot}$–$A^{-\cdot}$ state.[154] While usually, only one mechanism is active in producing the charge separation (CS), the charge recombination (CR) can involve both electron and hole transfer pathways, as schematically depicted in **Figure 9**.

Focusing on CISS, additional requirements on the nature of the photoexcited state on D or A apply. Simulations reported in Figure 4b,c are based on the assumption of a singlet photoexcited state. Though not strictly necessary, such an initial state simplifies the modeling of CISS. In some cases, the starting state can become crucial. In a first attempt to detect the CISS by trEPR some of us have investigated PET in CdSe quantum dots functionalized with oligopeptide chiral linkers terminated with the C_{60} acceptor group, as schematized in **Figure 10**a. The rationale behind this choice is that, on the one hand, CdSe QDs were already successfully employed to investigate CISS in PET, though only with indirect detection of spin polarization. On the other hand, RP formation was already detected in CdSe QDs coupled to NDI as an acceptor.[106] The spin properties of photogenerated $C_{60}^{-\cdot}$ radical anion are optimal due to the small spin–orbit coupling and the scarcity of magnetic nuclei. In the trEPR spectra reported in Figure 10b, the narrow signal superimposed to a broad signal due to the photoexcited triplet state of C_{60} is indicative of the formation of the $C_{60}^{-\cdot}$ radical anion.

According to the simulation of Figure 10d, the time evolution of this signal should in principle contain information on the spin selectivity of the PET process. Unfortunately, the experimental time evolution can only be reproduced assuming that the QD excited state is an admixture of singlet and triplet state. This is not surprising, given the large SO coupling of CdSe QDs promoting fast inter-system crossing (few picoseconds[106]) and the dimensions of the employed QDs resulting in a small singlet–triplet gap (few meV[155]). While both singlet and triplet initial states would result in pronounced differences in the Abs/Em features of the signal depending on whether CISS is included or not, the mixed

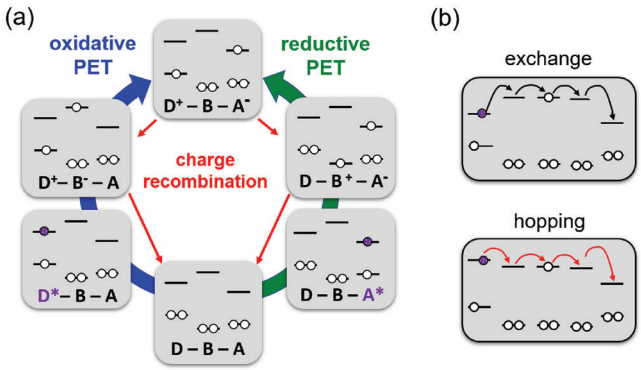

Figure 9. a) Schematic description of the processes leading to the charge-separated state after photoexcitation of the donor or the acceptor, where an electron or a hole is injected in the bridge, respectively. Both pathways can be involved in the charge recombination processes. b) Long-distance ET can occur either involving virtual states of the bridge in a multistep exchange mechanism (top) or real intermediate states in the hopping mechanism (bottom). The photoexcited state and electron are shown in purple.

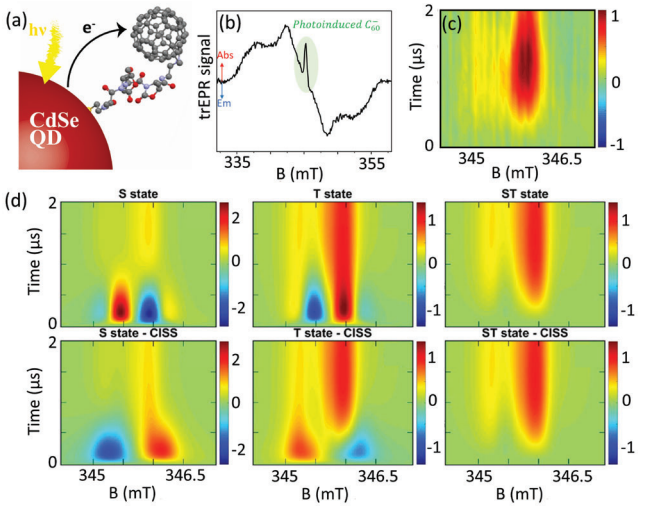

Figure 10. a) Schematic representation of the CdSe QD–χ–C_{60} system. The QD acts as an electron donor and C_{60} as an electron acceptor. The chiral bridge comprises the two-units peptidic chain (L-Ala-D-Oxd)$_2$, where D-Oxd=(4S,5R)-4-methyl-5-carboxyl-oxazolidin-2-one. b) trEPR spectrum taken at 1 μs after 450 nm laser pulse (7 ns, 2 mJ) acquired at 40 K. The spectrum shows a broad signal between 335–358 mT assigned to the C_{60} triplet and a narrow signal in enhanced absorption centered at ≈346 mT attributed to the photogenerated $C_{60}^{\bullet-}$ radical anion. Arrows legend: Abs = enhanced absorption, Em = emission. c) Time evolution of the trEPR signal of the C_{60} radical anion. d) Simulated time evolution assuming for the photoexcited QD the singlet (S), the triplet (T), or an admixture of singlet and triplet state (ST) computed without and with the spin filtering induced by CISS. Original data available in ref. [70].

state is completely insensitive, as shown in Figure 10c. The study has not allowed for discrimination of the presence of CISS and its spectroscopic quantification, thus evidencing the challenge of optimizing every single ingredient of the D–χ–A architecture. The previous example, though not at all conclusive on the presence of CISS in PET, has provided an important result. A CS state detectable through trEPR has been achieved using a long non-conjugated bridge. This leads us to the most critical ingredient, the chiral linker.

6.1.2. The Chiral Linker

The selection of the optimal linker is particularly challenging because of the currently incomplete understanding of the CISS phenomenon. As shown in ref. [110], a robust correlation between optical activity and spin filtering has been observed. Thus, it is not surprising that most CISS investigation involves oligopeptides of sizeable length (≈2 nm), where intramolecular H-bonds stabilize helical structures with enhanced circular dichroism signal. The same is true for supramolecular helicoidal aggregates.[110] Spin selective transport has been indeed observed also in supramolecular aggregates of achiral monomers where the chirality is imparted by the chiral solvent.[156] The availability of oligopeptide in enantiopure form, especially for the naturally occurring isomers, makes their use very convenient.

From these premises, a potential candidate for trEPR experiments to detect CISS-induced spin polarization could comprise pyrene, which is known to give PET from its long-lived excited singlet state, a good acceptor as C_{60} linked by oligopeptides. As an extension of the investigation summarized in Figure 10, different pyrene/C_{60} dyads with linkers comprising 4, 10, and 14 units, that is, alternating L-Ala and D-Oxd monomers were prepared.[157] Since it is known that ET rate can be influenced by the electric dipole moment of the molecule,[158] the options with Py and C_{60} on the C and N terminal end, that is, with dipole moment favoring the ET, and the reversed one have been investigated.

Despite some evidence of pyrene fluorescence quenching, trEPR investigations have not revealed any long-lived charge-separated state. This is in contrast with several observations of electron transport over distances well exceeding those investigated in the Py/C_{60} dyads.[159,160] Though attributed to the hopping mechanism, the weak temperature dependence of the transmission efficiency suggests that other mechanisms might contribute.[161] Indeed, CISS is expected to stabilize the RP state. As we have already mentioned, the forward ET is favored for a certain spin polarization of the electron, while the back ET will be likely suppressed for this spin state. Since spin relaxation is rather slow in organic radicals, this should lead to a prolonged lifetime of the RP state. This mechanism does not appear to be efficient enough to lead to photoinduced charge-separated states through oligopeptide bridges living long enough to be exploitable for the purposes presented in the previous sections. It is evident that the design criteria employed in electron transport are not directly transferrable to intramolecular PET. However, the results obtained with CdSe QD suggest that the target is not out of reach.

A subtle design of the linker can lead to separate control of the charge separation and recombination processes. A tutorial example is a case where the zinc porphyrin donor is linked to naphthoquinone by a rigid pentiptycene spacer.[162] Modifying a substituent on the linker from OMe to H makes the linker less prone to oxidation. According to the scheme of Figure 9, the D–$B^{+\cdot}$–$A^{-\cdot}$ state is only involved in the CR process. Thus, such a replacement selectively reduces the efficiency of the back electron transfer without affecting the forward process. The addition of intermediate A/D along the linker has also demonstrated to be very efficient for the production of long-lived RPs.[52,163–165] The introduction of a chiral element in such optimized linkers might represent a valid alternative to helicoidal structures, though the CISS efficiency in electron transport when chirality is not spatially extended is still to be assessed.

Alternative approaches might involve conjugated chiral linkers of the helicene type, where chirality is achieved in the absence of a stereogenic center.[166] The racemization barrier increases dramatically with the number of rings, allowing for the separation of pure enantiomers and their retention upon derivatization or self-assembly procedures. Heteroatoms can be inserted in the scaffold providing a huge variety of properties. Focusing on CISS-related experiments, helicene-based molecules are attracting increasing interest because of their strong optical rotatory efficiency and their good electron transmission in spintronics devices.[114,167] Spin-dependent photoemission was observed from metal surfaces on which a monolayer of [7]helicene molecules was deposited.[117] Thiadiazole–helicene molecules adsorbed on electrodes have also been demonstrated to enhance the catalytic activity in oxygen-evolving reactions,[168] similar to what was observed with DNA and oligopeptides.[169] Despite the rich chemistry in the functionalization of helicene scaffolds,

mainly aimed at improving their chiroptical properties, such as the emission of circularly polarized light,[170] PET leading to long-lived RP states in helicenes is, to the best of our knowledge, still unreported.

6.1.3. The Qubit

The qubit appears as the less critical building block of the proposed architectures. More than a decade of research has led to significant achievements, some of them summarized in Table 1 and discussed in several reviews.[1–3] Coherence times of the order of 10 µs at liquid helium or 1 µs at room temperature are easily achieved either in organic radicals,[171] graphenoids,[172] or metal complexes,[13,30] particularly if orbital contributions are minimized.[10,12,173] This would already allow the implementation of many quantum operations before losing coherence and operating at rather high temperatures, where CISS is more efficient, even if good spin filtering has been observed also at 4 K.[174]

Although the coherence time is not the current limiting factor, it could be further enhanced, by controlling both the nuclear spin bath[8,11] (which drives low-temperature decoherence) and phonon-mediated relaxation and dephasing processes (which dominate at rather high temperatures). This can be done through a careful design of the molecular structure (coordination geometry, ligand rigidity), electronic gaps and spin–phonon couplings, as suggested for instance in refs. [175–179].

The first experiments involving a paramagnetic species coupled to an A/D dyad and demonstrating spin teleportation after PET[97] involve the well-known Koelsch organic radical, that is, 1,3-bisdiphenylene-2-phenylallyl (BDPA).[180] More recently, also the (2,2,6,6-tetramethylpiperidin-1-yl)oxyl or (2,2,6,6-tetramethylpiperidin-1-yl)oxidanyl (TEMPO) radical has been employed.[181] The same Koelsch radical, linked to a fullerene moiety, has been recently used to demonstrate that the photogenerated triplet state of C_{60} can be used to transfer spin polarization on the radical.[182] Carbon-based radicals have the advantage of long T_2 and narrow spectra with only weak hyperfine splitting, further reduced by deuteration. Biradical species have also been employed to implement quantum gates.[183]

Despite the remarkable results obtained with organic radicals, coordination compounds present features that can be relevant for implementing the proposed architectures. The first advantage is the more pronounced deviation of g from the free-electron value separating the qubit magnetic resonance from those of the photoinduced RP, as shown in Figure 4e. Addressability of individual spins is even more crucial in the design of two-qubit gates. Heterometallic compounds are a natural choice, as in a recent example comprising Cu^{2+} and Ti^{3+} $S = 1/2$ centers.[184] However, homometallic complexes can also be employed, provided that the two identical g-tensors are not parallel. If the deviations from $g = 2$ are small, as in the case of the best-performing molecular spin qubits, the anisotropy and non-collinearity of the hyperfine interaction can be harnessed, as demonstrated for the weakly exchanged coupled vanadyl–porphyrin dimer reported in Table 1.[23]

Hyperfine interactions also deserve further comment. The coherence of the electronic spin is mainly limited at low temperature by weakly coupled nuclear spins of the ligands and the solvent.[185,186] When working on a spin ensemble, nuclear spin levels are considerably more demanding to initialize than electron spin levels. However, at the single molecule level, the nuclear spin of the paramagnetic ion can be an important resource for quantum information. As already shown in Table 1, the $I = 3/2$ nuclear spin of terbium in the $TbPc_2$ molecule has been used to implement the Grover algorithm .[187] The large nuclear quadrupolar splitting has been key to addressing individual nuclear resonances. Interestingly, quadrupolar splitting is not indispensable for this purpose. When operating at reasonably low magnetic fields, the hyperfine anisotropy acts as an effective quadrupolar splitting, as demonstrated in single crystal broadband NMR experiments of some vanadium(IV) complexes.[18,188]

Playing with such a flexible and programmable multitude of levels of coordination compounds is very appealing, but integrating these relatively fragile objects in the D/A dyads is not straightforward. Chemically robust and rigid coordination environments, as in porphyrin compounds,[23,189,190] allow for retaining the spin properties of the qubit once attached to the molecular scaffold of the dyad. The non-innocent photochemical behavior of these ligands is a wild card that deserves to be explored.

6.2. Toward Devices

The second step toward the implementation of spin-to-charge conversion based on CISS necessitates a device architecture that has been poorly explored so far. Most existing spintronic devices are primarily based on spin currents serving as a transmitter of information from the injector to the detector or as a carrier of angular momentum for magnetization switching applications. In view of quantum technology applications and the need to retain the coherence of the spin system, we have envisaged a different platform relying on the field-effect transistor (FET) architecture. The following section does not purport to be exhaustive and/or to discuss the multitude of possible CISS-based readout devices that can be envisaged. We will only limit ourselves to giving some tentative architectures that can be adopted to implement CISS-based readout of molecular qubits in real devices.

6.2.1. Single-Electron Transistor

The basic idea of our detection scheme is presented in Section 5.2 and comprises the use of the potential generated by the CS state of the dyad as the gating bias of a FET device. In this regard, single-electron transistors (SETs) are a promising architecture for achieving exceptional detection sensitivity.[191] Specifically, for high-precision electrometry, a two-gate SET could be used.[192] The first gate is the usual bias while the second one is generated by the dyad exhibiting CISS-controlled ET. To achieve maximum sensitivity, the bias voltage of the first gate is kept close to the Coulomb blockade voltage. In this way, the generation of a photoinduced CS state in the CISS-based dyad will produce a significant variation in the conductance of SET. In this sense, the SET is considered a highly sensitive, miniaturized electrometer, which can easily sense a fraction of the elementary (sub-single-electron) charge by the change in its characteristics.

A key problem of this device is that low temperatures are required to achieve single electron operation since the thermal

energy must be lower than the charging energy of the island.[193] Nevertheless, operations at low temperatures hinder the unique advantage of the CISS effect, which might allow room temperature operations. A first solution is to increase the charging energy of the island above $k_B T$ by reducing the island dimension (less than 10 nm). The recent advancements in lithographic techniques for the fabrication of ultrasmall islands have already allowed the realization of SET devices that operate at room temperature.[194,195] These devices are based on FinFET channels with a steeply etched trench in the center and oxidation-induced strain. Although their reproducibility is still low, these silicon-based technologies hold great potential in view of large-scale production of room-temperature SET.

Implementation of multiple-tunnel junctions (MTJs),[196] that is, formed by a chain of nanoscale islands linked with tunnel junctions, is another promising means of increasing the charging energy for room temperature operation. A promising example of this approach has been recently demonstrated by the realization of robust and well-controlled MTJ architectures of germanium nanoparticles rooted by a germanium oxide ropeway. These MTJ devices fabricated via a cost-effective, template-free, and scalable vapor transport method have shown an ideal Coulomb staircase behavior of single-electron charge transfer at room temperature. Importantly, the chemical tunability of the island, for example, by using different island and tunneling barrier materials, coupled with the flexibility of lithography allows the fine control not only of the charging energy but also other key parameters, for example, coherence times, transport properties, electron tunneling rate Γ.[197] In this regard, across the years, a large variety of materials have been tested ranging from the initial GaAs/AlGaAs heterostructures to the state-of-the-art Si/SiGe heterostructures and Si metal–oxide–semiconductor (MOS) architectures,[137] from metal nanoparticles[198] to carbon allotropes.[199,200]

6.2.2. Field-Effect Transistor

SETs have high sensitivities but require advanced lithographic capabilities and the deposition of one D–χ–A–Q unit on the SET for single spin readout, see Figure 6. Relevant proof-of-principle experiments can be realized by adopting a simple organic FET (OFET) architecture embedding a small ensemble of molecules constituting a dense monolayer deposit. OFETs stand out as one of the most used platforms for the construction of inexpensive, adaptable, and lightweight devices, for example, for sensing[201] and data storage.[202]

In an operating OFET, high density of the charge carriers is confined to few molecular layers adjacent to the interface with the dielectric. Thus, a small change in this interface can induce significant modulations of the device's electrical characteristics. In particular, it has been shown that photochromic molecules embedded at the semiconductor/dielectric interface can form a layer, known as floating-gate interlayer,[202–204] through which the OFET can be operated. The organic photochromic compound acts as a molecular trigger that can be modulated using various optoelectrical programming regimes to enable the operation of advanced organic memory elements. Such devices have demonstrated excellent write–read–erase cycling endurance and data retention times.

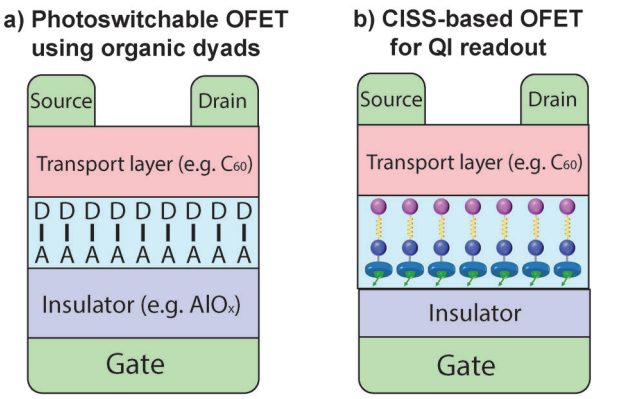

Figure 11. Schematic layout of the device architectures incorporating a SAM of photosensitive D/A dyads. a) Layout fabricated and characterized in ref. [205] based on porphyrin–fullerene dyads anchored to AlOx through carboxylic groups. b) Exemplary OFET device proposed for the spin-to-charge conversion based on CISS effect. Here the gate voltage can be used to promote charge recombination as an alternative to light, as discussed in Section 5.

Along this line, very recent work has demonstrated that monolayers of D/A porphyrin–fullerene dyads can act as light-responsive triggers modulating the electrical characteristics of OFETs (**Figure 11**a).[205] The operational mechanism of these devices has been described as follows. After the absorption of photons by D, photoinduced ET from D to A occurs, thereby generating a CS state. In the writing step, the gate voltage is driven so that some electrons jump from the fullerene to the AlOx layer where they get trapped. Switching off the light results in intramolecular recombination of positive and negative charges except for the dyads which have lost their electrons. These dyads keep positive charges on the porphyrin units thereby turning on the OFET transport layer. In the erasing step, an opposite gate voltage is applied under light irradiation so that the holes can jump from the porphyrin to the AlOx layer. During this step, the previously AlOx-trapped electrons are neutralised. This is just an example of the great potential that organic D/A dyads can have in the field of OFET architectures. It demonstrates that the CS state of the dyad can be electrically detected and appears promising for the utilization of CISS-based dyads as spin-to-charge converters.

In our CISS-based proposal, we do not want to store long-lived information but rather detect the spin polarization of the qubit after mw operations. This can be done by self-assembling a monolayer of D–χ–A–Q unit in the OFET device, as schematized in Figure 11b). Following light excitation, the photoinduced electron transfer generates spin-polarized CS states, which turn on the OFET channel. Recalling what has been presented in Section 5, the spin-polarized CS state can be used to initialize the qubit (see Figure 5b). After qubit manipulations, the quantum information can be swapped back to the acceptor spin and charge recombination induced by light or gate voltage. Thanks to CISS, the spin state of the acceptor affects this recombination (see Figure 6c,d). As a consequence, the resulting charge in the donor layer, acting as the OFET floating gate, is representative of the spin state of the qubit layer.

For our purposes, qubit manipulation requires that the OFET is coupled with microwaves. This combination is not

unprecedented as it is the basis of electrically detected magnetic resonance (EDMR). EDMR is a technique used to enhance the sensitivity of magnetic resonance by replacing the detection of microwave quanta by a much more sensitive current measurement.[206–210] It is generally applicable for systems with spin-dependent currents and thus susceptible to spin manipulation by EPR. The technique has been extensively used in the study of silicon materials, for example, photovoltaic devices, and has been suggested as a potential scheme to readout coherent spin states of quantum bits in the semiconductor-based quantum computer concept.[211]

The OFET approach discussed above[205] is here extended to qubit measurements with separation between the qubit states and the charge carriers, allowing retention of the spin coherence properties of molecular qubits. One challenge for implementing this readout scheme is the OFET detection of the electric dipole field of the CT state instead of the full charge of a memory element. The considerable distance between the donor and the acceptor separated by the chiral bridge and the availability of opportune strategies to enhance sensitivity[212,213] make this approach promising.

7. Conclusions

To summarize, we have shown that chiral-induced spin selectivity could be a valuable enabling technology for quantum applications. In particular, we have proposed a scheme exploiting CISS at the molecular level to initialize, process, and readout the states of molecular spin qubits and qudits.

Combining CISS with photons in superconducting resonators[4] could provide a promising route toward the scalability of the device. This appears technologically feasible, thanks to the power of chemical design and the capability of organizing molecules on superconducting surfaces. It would allow exploiting the best properties of both architectures. On the one hand, CISS would enable manipulations and read-out of single molecules. On the other hand, the mobility of photons could be exploited to implement two-qubit gates and establish entanglement between distant qubits.

The actual realization of the molecular setup here proposed for quantum applications requires preliminary targeted experiments to finally elucidate the nature of CISS. As discussed in this paper, this simplified setup gets rid of interfaces and cooperative effects and allows one to focus on the role of chirality, thus achieving a deeper theoretical understanding of the phenomenon. Indeed, a full tomography of the spin state of the transferred electron would provide the information needed to guide theoretical modeling.

An important point for quantum technology applications is related to the temperature dependence of the CISS effect and to the possibility of tuning it by engineering the molecular structure. Indeed, recent results suggest that CISS efficiency increases with temperature whereas coherence times of molecular qubits typically decrease. However, coherent manipulations of molecular qubits had been performed even at room temperature. This temperature resilience could be further increased by engineering ligands and removing neighboring nuclear spins. Moreover, very high spin polarization was mostly found so far on 2D materials such as chiral hybrid lead-iodide perovskites,[111] hybrid copper halides,[112] or MOFs.[113] Further investigations in molecular systems are thus needed. Finally, the present proposal is based on a simple hypothesis on the CISS effect in electron transfer and recombination processes,[68] which should be confirmed by targeted experiments. In fact, CISS had already been demonstrated in electron transfer, but its precise characteristics and efficiency in the proposed setup still need to be assessed. Nonetheless, our proposal could be adapted once direct experimental results on electron transfer through a chiral bridge at the molecular scale are available.

Acknowledgements

This *Perspective* stems from stimulating discussions with many colleagues. In particular, Mario Chiesa, Andrea Cornia, Francesco Pineider, Enrico Salvadori, Claudia Tomasini, and Jan Behrends are heartily acknowledged. This work has received funding from the Italian Ministry of University and Research (MUR), through PRIN Project 2017CR5WCH Q-chiSS "Quantum detection of chiral-induced spin selectivity at the molecular level" and through Dipartimenti di Eccellenza 2023-2027 (DICUS 2.0) to the Department of Chemistry "Ugo Schiff" of the University of Florence, from the European Unions Horizon 2020 research and innovation programme (FET-OPEN project FATMOLS) under grant agreement no. 862893, and from Fondazione Cariparma. Project funded under the National Recovery and Resilience Plan (NRRP), Mission 4 Component 2 Investment 1.3 - Call for tender No. 341 of 15/03/2022 of Italian Ministry of University and Research funded by the European Union – NextGenerationEU, award number PE0000023, Concession Decree No. 1564 of 11/10/2022 adopted by the Italian Ministry of University and Research, CUP D93C22000940001, Project title "National Quantum Science and Technology Institute" (NQSTI). A.P. acknowledges funding by the Italian Ministry of University and Research (MUR) under the National Recovery and Resilience Plan (NRRP), Mission 4 Component 2 Investment 1.2 - Call for tender No. 247 of 19/08/2022 (Project ID: SOE_0000064, Photodriven spin selectivity in chiral organic molecules and devices - PHOTOCODE). This work was also supported by the US National Science Foundation under Award no. CHE-2154627 (M.R.W.) This perspective represents the vision of the ERC-Synergy project CASTLE (proj. n. 101071533) funded by the Horizon Europe Programme, which is also acknowledged.

Open Access Funding provided by Universita degli Studi di Firenze within the CRUI-CARE Agreement.

Conflict of Interest

The authors declare no conflict of interest.

Keywords

chirality-induced spin selectivity, electron transfer, magnetic resonances, molecular nanomagnets, quantum computing

Received: January 15, 2023
Revised: February 21, 2023
Published online: May 12, 2023

[1] A. Gaita-Ariño, F. Luis, S. Hill, E. Coronado, *Nat. Chem.* **2019**, *11*, 301.
[2] M. Atzori, R. Sessoli, *J. Am. Chem. Soc.* **2019**, *141*, 11339.
[3] M. R. Wasielewski, M. D. E. Forbes, N. L. Frank, K. Kowalski, G. D. Scholes, J. Yuen-Zhou, M. A. Baldo, D. E. Freedman, R. H. Goldsmith, T. Goodson, M. L. Kirk, J. K. McCusker, J. P. Ogilvie, D. A. Shultz, S. Stoll, K. B. Whaley, *Nat. Rev. Chem.* **2020**, *4*, 490.

[4] S. Carretta, D. Zueco, A. Chiesa, A. Gómez-León, F. Luis, *Appl. Phys. Lett.* **2021**, *118*, 240501.
[5] A. J. Heinrich, W. D. Oliver, L. M. K. Vandersypen, A. Ardavan, R. Sessoli, D. Loss, A. Bleszynski Jayich, J. Fernandez-Rossier, L. A., A. Morello, *Nat. Nanotechnol.* **2021**, *16*, 1318.
[6] C. J. Wedge, G. A. Timco, E. T. Spielberg, R. E. George, F. Tuna, S. Rigby, E. J. L. McInnes, R. E. P. Winpenny, S. J. Blundell, A. Ardavan, *Phys. Rev. Lett.* **2012**, *108*, 107204.
[7] M. Shiddiq, D. Komijani, Y. Duan, A. Gaita-Ariño, E. Coronado, S. Hill, *Nature* **2016**, *531*, 348.
[8] J. M. Zadrozny, J. Niklas, O. G. Poluektov, D. E. Freedman, *ACS Cent. Sci.* **2015**, *1*, 488.
[9] J. Zadrozny, D. E. Freedman, *Inorg. Chem.* **2015**, *54*, 12027.
[10] M. J. Graham, J. M. Zadrozny, M. Shiddiq, J. S. Anderson, M. S. Fataftah, S. Hill, D. E. Freedman, *J. Am. Chem. Soc.* **2014**, *136*, 7623.
[11] C.-J. Yu, M. J. Graham, J. M. Zadrozny, J. Niklas, M. D. Krzyaniak, M. R. Wasielewski, O. G. Poluektov, D. E. Freedman, *J. Am. Chem. Soc.* **2016**, *138*, 14678.
[12] M. Atzori, E. Morra, L. Tesi, A. Albino, M. Chiesa, L. Sorace, R. Sessoli, *J. Am. Chem. Soc.* **2016**, *138*, 11234.
[13] M. Atzori, L. Tesi, E. Morra, M. Chiesa, L. Sorace, R. Sessoli, *J. Am. Chem. Soc.* **2016**, *138*, 2154.
[14] M. Atzori, L. Tesi, S. Benci, A. Lunghi, R. Righini, A. Taschin, R. Torre, L. Sorace, R. Sessoli, *J. Am. Chem. Soc.* **2017**, *139*, 4338.
[15] M. Atzori, S. Benci, E. Morra, L. Tesi, M. Chiesa, R. Torre, L. Sorace, R. Sessoli, *Inorg. Chem.* **2018**, *57*, 731.
[16] L. Tesi, E. Lucaccini, I. Cimatti, M. Perfetti, M. Mannini, M. Atzori, E. Morra, M. Chiesa, A. Caneschi, L. Sorace, R. Sessoli, *Chem. Sci.* **2016**, *7*, 2074.
[17] R. Hussain, G. Allodi, A. Chiesa, E. Garlatti, D. Mitcov, A. Konstantatos, K. Pedersen, R. D. Renzi, S. Piligkos, S. Carretta, *J. Am. Chem. Soc.* **2018**, *140*, 9814.
[18] S. Chicco, A. Chiesa, G. Allodi, M. Garlatti, E. Atzori, L. Sorace, R. De Renzi, R. Sessoli, S. Carretta, *Chem. Sci.* **2021**, *12*, 12046.
[19] J. Liu, J. Mrozek, A. Ullah, Y. Duan, J. J. Baldoví, E. Coronado, A. Gaita-Ariño, A. Ardavan, *Nat. Phys.* **2021**, *17*, 1205.
[20] A. Ardavan, A. M. Bowen, A. Fernandez, A. J. Fielding, D. Kaminski, F. Moro, C. A. Muryn, M. D. Wise, A. Ruggi, E. J. L. McInnes, K. Severin, G. A. Timco, C. R. Timmel, F. Tuna, G. F. S. Whitehead, R. E. P. Winpenny, *npj Quantum Inf.* **2015**, *1*, 15012.
[21] D. Aguilà, D. Barrios, V. Velasco, O. Roubeau, A. Repollés, P. Alonso, J. Sesé, S. Teat, F. Luis, G. Aromí, *J. Am. Chem. Soc.* **2014**, *136*, 14215.
[22] J. Ferrando-Soria, E. Moreno-Pineda, A. Chiesa, A. Fernandez, S. A. Magee, S. Carretta, P. Santini, I. Vitorica-Yrezabal, F. Tuna, E. J. L. McInness, R. E. P. Winpenny, *Nat. Commun.* **2016**, *7*, 11377.
[23] D. Ranieri, F. Santanni, A. Privitera, A. Albino, E. Salvadori, M. Chiesa, F. Totti, L. Sorace, R. Sessoli, *Chem. Sci.* **2023**, *14*, 61.
[24] A. Chiesa, G. F. S. Whitehead, S. Carretta, L. Carthy, G. A. Timco, S. J. Teat, G. Amoretti, E. Pavarini, R. E. P. Winpenny, P. Santini, *Sci. Rep.* **2014**, *4*, 7423.
[25] J. Ferrando-Soria, S. A. Magee, A. Chiesa, S. Carretta, P. Santini, I. J. Vitorica-Yrezabal, F. Tuna, G. F. S. Whitehead, S. Sproules, K. M. Lancaster, A.-L. Barra, G. A. Timco, E. J. L. McInnes, R. E. P. Winpenny, *Chem* **2016**, *1*, 727.
[26] M. Atzori, A. Chiesa, E. Morra, M. Chiesa, L. Sorace, S. Carretta, R. Sessoli, *Chem. Sci.* **2018**, *9*, 6183.
[27] S. J. Lockyer, A. Chiesa, A. Brookfield, G. A. Timco, G. F. S. Whitehead, E. J. L. McInnes, S. Carretta, R. E. P. Winpenny, *J. Am. Chem. Soc.* **2022**, *144*, 16086.
[28] C. Godfrin, A. Ferhat, R. Ballou, S. Klyatskaya, M. Ruben, W. Wernsdorfer, F. Balestro, *Phys. Rev. Lett.* **2017**, *119*, 187702.
[29] E. Moreno-Pineda, C. Godfrin, F. Balestro, W. Wernsdorfer, M. Ruben, *Chem. Soc. Rev.* **2018**, *47*, 501.
[30] K. Bader, D. Dengler, S. Lenz, B. Endeward, S.-D. Jiang, P. Neugebauer, J. van Slageren, *Nat. Commun.* **2014**, *5*, 5304.
[31] G. A. Timco, S. Carretta, F. Troiani, F. Tuna, R. J. Pritchard, C. A. Muryn, E. J. L. McInnes, A. Ghirri, A. Candini, P. Santini, G. Amoretti, M. Affronte, R. E. P. Winpenny, *Nat. Nanotechnol.* **2009**, *4*, 173.
[32] A. Chiesa, E. Macaluso, F. Petiziol, S. Wimberger, P. Santini, S. Carretta, *J. Phys. Chem. Lett.* **2020**, *11*, 8610.
[33] E. Macaluso, M. Rubín, D. Aguilà, A. Chiesa, J. I. M. L. A. Barrios, P. J. Alonso, O. Roubeau, F. Luis, G. Aromí, S. Carretta, *Chem. Sci.* **2020**, *11*, 10337.
[34] A. Chiesa, F. Petiziol, M. Chizzini, P. Santini, S. Carretta, *J. Phys. Chem. Lett.* **2022**, *13*, 6468.
[35] A. Cornia, M. Mannini, P. Sainctavit, R. Sessoli, *Chem. Soc. Rev.* **2011**, *40*, 3076.
[36] B. W. Heinrich, L. Braun, J. I. Pascual, K. J. Franke, *Nat. Phys.* **2013**, *9*, 765.
[37] L. Malavolti, M. Briganti, M. Hänze, G. Serrano, I. Cimatti, G. McMurtrie, E. Otero, P. Ohresser, F. Totti, M. Mannini, R. Sessoli, S. Loth, *Nano Lett.* **2018**, *18*, 7955.
[38] G. Serrano, L. Poggini, M. Briganti, A. L. Sorrentino, G. Cucinotta, L. Malavolti, B. Cortigiani, E. Otero, P. Sainctavit, S. Loth, F. Parenti, A.-L. Barra, A. Vindigni, A. Cornia, F. Totti, M. Mannini, R. Sessoli, *Nat. Mater.* **2020**, *19*, 546.
[39] S. M. F. Shahed, F. Ara, M. I. Hossain, K. Katoh, M. Yamashita, T. Komeda, *ACS Nano* **2022**, *16*, 7651.
[40] M. Briganti, G. Serrano, L. Poggini, A. L. Sorrentino, B. Cortigiani, L. C. de Camargo, J. F. Soares, A. Motta, A. Caneschi, M. Mannini, F. Totti, R. Sessoli, *Nano Lett.* **2022**, *22*, 8626.
[41] C. Bonizzoni, A. Ghirri, F. Santanni, M. Atzori, L. Sorace, R. Sessoli, M. Affronte, *npj Quantum Inf.* **2020**, *6*, 68.
[42] V. Rollano, M. C. de Ory, C. D. Buch, M. Rubín-Osanz, D. Zueco, C. Sánchez-Azqueta, A. Chiesa, D. Granados, S. Carretta, A. Gomez, S. Piligkos, F. Luis, *Commun. Phys.* **2022**, *5*, 246.
[43] S. Schulte, N. Néel, L. Rózsa, K. Palotás, J. Kröger, *Nano Lett.* **2023, 23, 162**.
[44] J. O. Island, R. Gaudenzi, J. de Bruijckere, E. Burzurí, C. Franco, M. Mas-Torrent, C. Rovira, J. Veciana, T. M. Klapwijk, R. Aguado, H. S. J. van der Zant, *Phys. Rev. Lett.* **2017**, *118*, 117001.
[45] F. Tacchino, A. Chiesa, R. Sessoli, I. Tavernelli, S. Carretta, *J. Mater. Chem. C* **2021**, *9*, 10266.
[46] I. Gimeno, A. Urtizberea, J. Román-Roche, D. Zueco, A. Camón, P. J. Alonso, O. Roubeau, F. Luis, *Chem. Sci.* **2021**, *12*, 5621.
[47] M. Chizzini, L. Crippa, A. Chiesa, F. Tacchino, F. Petiziol, I. Tavernelli, P. Santini, S. Carretta, *Phys. Rev. Res.* **2022**, *4*, 043135.
[48] F. Petiziol, A. Chiesa, S. Wimberger, P. Santini, S. Carretta, *npj Quantum Inf.* **2021**, *7*, 133.
[49] M. Chizzini, L. Crippa, L. Zaccardi, E. Macaluso, S. Carretta, A. Chiesa, P. Santini, *Phys. Chem. Chem. Phys.* **2022**, *24*, 20030.
[50] S. L. Bayliss, D. W. Laorenza, P. J. Mintun, B. D. Kovos, D. E. Freedman, D. D. Awschalom, *Science* **2020**, *370*, 1309.
[51] D. W. Laorenza, D. E. Freedman, *J. Am. Chem. Soc.* **2022**, *144*, 21810.
[52] S. M. Harvey, M. R. Wasielewski, *J. Am. Chem. Soc.* **2021**, *143*, 15508.
[53] R. Naaman, Y. Paltiel, D. H. Waldeck, *Nat. Rev. Chem.* **2019**, *3*, 250.
[54] R. Naaman, Y. Paltiel, D. H. Waldeck, *J. Phys. Chem. Lett.* **2020**, *11*, 3660.
[55] R. Naaman, Y. Paltiel, D. H. Waldeck, *Acc. Chem. Res.* **2020**, *53*, 2659.
[56] C. D. Aiello, J. M. Abendroth, M. Abbas, A. Afanasev, S. Agarwal, A. S. Banerjee, D. N. Beratan, J. N. Belling, B. Berche, A. Botana, J. R. Caram, G. L. Celardo, G. Cuniberti, A. Garcia-Etxarri, A. Dianat, I. Diez-Perez, Y. Guo, R. Gutierrez, C. Herrmann, J. Hihath, S. Kale, P. Kurian, Y.-C. Lai, T. Liu, A. Lopez, E. Medina, V. Mujica, R. Naaman, M. Noormandipour, J. L. Palma, et al., *ACS Nano* **2022**, *16*, 4989.
[57] A. Forment-Aliaga, A. Gaita-Ariño, *J. Appl. Phys.* **2022**, *132*, 180901.

[58] E. Z. B. Smolinsky, A. Neubauer, A. Kumar, S. Yochelis, E. Capua, R. Carmieli, Y. Paltiel, R. Naaman, K. Michaeli, *J. Phys. Chem. Lett.* **2019**, *10*, 1139.
[59] S. Ghosh, S. Mishra, E. Avigad, B. P. Bloom, L. T. Baczewski, S. Yochelis, Y. Paltiel, R. Naaman, D. H. Waldeck, *J. Phys. Chem. Lett.* **2020**, *11*, 1550.
[60] K. Banerjee-Ghosh, O. Ben Dor, F. Tassinari, E. Capua, S. Yochelis, A. Capua, S.-H. Yang, S. S. P. Parkin, S. Sarkar, L. Kronik, L. T. Baczewski, R. Naaman, Y. Paltiel, *Science* **2018**, *360*, 1331.
[61] A. C. Aragonès, E. Medina, M. Ferrer-Huerta, N. Gimeno, M. Teixidó, J. L. Palma, N. Tao, J. M. Ugalde, E. Giralt, I. Díez-Pérez, V. Mujica, *Small* **2017**, *13*, 1602519.
[62] I. Carmeli, K. S. Kumar, O. Heifler, C. Carmeli, R. Naaman, *Angew. Chem., Int. Ed.* **2014**, *53*, 8953.
[63] F. Evers, A. Aharony, N. Bar-Gill, O. Entin-Wohlman, P. Hedegård, O. Hod, P. Jelinek, G. Kamieniarz, M. Lemeshko, K. Michaeli, V. Mujica, R. Naaman, Y. Paltiel, S. Refaely-Abramson, O. Tal, J. Thijssen, M. Thoss, J. M. van Ruitenbeek, L. Venkataraman, D. H. Waldeck, B. Yan, L. Kronik, *Adv. Mater.* **2022**, *34*, 2106629.
[64] J. Fransson, *J. Phys. Chem. Lett.* **2019**, *10*, 7126.
[65] J. Fransson, *Phys. Rev. B* **2020**, *102*, 235416.
[66] J. Fransson, *Nano Lett.* **2021**, *21*, 3026.
[67] T. P. Fay, *J. Phys. Chem. Lett.* **2021**, *12*, 1407.
[68] J. Luo, P. J. Hore, *New J. Phys.* **2021**, *23*, 043032.
[69] A. Chiesa, M. Chizzini, E. Garlatti, E. Salvadori, F. Tacchino, P. Santini, I. Tavernelli, R. Bittl, M. Chiesa, R. Sessoli, S. Carretta, *J. Phys. Chem. Lett.* **2021**, *12*, 6341.
[70] A. Privitera, E. Macaluso, A. Chiesa, A. Gabbani, D. Faccio, D. Giuri, M. Briganti, N. Giaconi, F. Santanni, N. Jarmouni, L. Poggini, M. Mannini, M. Chiesa, C. Tomasini, F. Pineider, E. Salvadori, S. Carretta, R. Sessoli, *Chem. Sci.* **2022**, *13*, 12208.
[71] D. P. DiVincenzo, *Fortschr. Phys.* **2000**, *48*, 771.
[72] R. A. Marcus, *J. Chem. Phys.* **1956**, *24*, 966.
[73] R. A. Marcus, *J. Chem. Phys.* **1965**, *43*, 679.
[74] N. S. Hush, *J. Chem. Phys.* **1958**, *28*, 962.
[75] J. Ulstrup, J. Jortner, *J. Chem. Phys.* **1975**, *63*, 4358.
[76] A. Weller, *Z. Phys. Chem.* **1982**, *133*, 93.
[77] M. C. Thurnauer, J. R. Norris, *Chem. Phys. Lett.* **1980**, *76*, 557.
[78] G. L. Closs, M. D. E. Forbes, J. R. Norris, *J. Phys. Chem.* **1987**, *91*, 3592.
[79] C. Buckley, D. Hunter, P. Hore, K. McLauchlan, *Chem. Phys. Lett.* **1987**, *135*, 307.
[80] D. Stehlik, C. H. Bock, J. Petersen, *J. Phys. Chem.* **1989**, *93*, 1612.
[81] R. Bittl, A. van der Est, A. Kamlowski, W. Lubitz, D. Stehlik, *Chem. Phys. Lett.* **1994**, *226*, 349.
[82] For exceptions making use of recombination luminescence see, for example, the review [83], or [84,85].
[83] V. A. Bagryansky, V. I. Borovkov, Y. N. Molin, *Russ. Chem. Rev.* **2007**, *76*, 493.
[84] P. Gilch, F. Pällinger-Dammer, C. Musewald, M. E. Michel-Beyerle, U. E. Steiner, *Science* **1998**, *281*, 982.
[85] D. Mims, J. Herpich, N. N. Lukzen, U. E. Steiner, C. Lambert, *Science* **2021**, *374*, 1470.
[86] K. M. Salikhov, C. H. Bock, D. Stehlik, *Appl. Magn. Reson.* **1990**, *1*, 195.
[87] K. M. Salikhov, Y. E. Kandrashkin, A. K. Salikhov, *Appl. Magn. Reson.* **1992**, *3*, 199.
[88] E. Goovaerts, *eMagRes* **2017**, *6*, 343.
[89] S. S. Kim, S. Weissman, *J. Magn. Reson. (1969)* **1976**, *24*, 167.
[90] S. Weber, in *Transient EPR*, Wiley, New York **2017**, pp. 255–270.
[91] S. A. Dzuba, P. Gast, A. J. Hoff, *Chem. Phys. Lett.* **1995**, *236*, 595.
[92] R. Bittl, S. G. Zech, *J. Phys. Chem. B* **1997**, *101*, 1429.
[93] R. Bittl, G. Kothe, *Chem. Phys. Lett.* **1991**, *177*, 547.
[94] G. Kothe, S. Weber, R. Bittl, E. Ohmes, M. C. Thurnauer, J. R. Norris, *Chem. Phys. Lett.* **1991**, *186*, 474.
[95] K. Laukenmann, S. Weber, G. Kothe, C. Oesterle, A. Angerhofer, M. R. Wasielewski, W. A. Svec, J. R. Norris, *J. Phys. Chem.* **1995**, *99*, 4324.
[96] S. Pirandola, J. Eisert, C. Weedbrook, A. Furusawa, S. L. Braunstein, *Nat. Photonics* **2015**, *9*, 641.
[97] B. K. Rugg, M. D. Krzyaniak, B. T. Phelan, M. A. Ratner, R. M. Young, M. R. Wasielewski, *Nat. Chem.* **2019**, *11*, 981.
[98] B. K. Rugg, K. E. Smyser, B. Fluegel, C. H. Chang, K. J. Thorley, S. Parkin, J. E. Anthony, J. D. Eaves, J. C. Johnson, *Proc. Natl. Acad. Sci. USA* **2022**, *119*, e2201879119.
[99] N. E. Horwitz, B. T. Phelan, J. N. Nelson, M. D. Krzyaniak, M. R. Wasielewski, *J. Phys. Chem. A* **2016**, *120*, 2841.
[100] N. E. Horwitz, B. T. Phelan, J. N. Nelson, C. M. Mauck, M. D. Krzyaniak, M. R. Wasielewski, *J. Phys. Chem. A* **2017**, *121*, 4455.
[101] M. T. Colvin, R. Carmieli, T. Miura, S. Richert, D. M. Gardner, A. L. Smeigh, S. M. Dyar, S. M. Conron, M. A. Ratner, M. R. Wasielewski, *J. Phys. Chem. A* **2013**, *117*, 5314.
[102] Q. Mi, E. T. Chernick, D. W. McCamant, E. A. Weiss, M. A. Ratner, M. R. Wasielewski, *J. Phys. Chem. A* **2006**, *110*, 7323.
[103] J. N. Nelson, J. Zhang, J. Zhou, B. K. Rugg, M. D. Krzyaniak, M. R. Wasielewski, *J. Chem. Phys.* **2020**, *152*, 014503.
[104] S. Nakazawa, S. Nishida, T. Ise, T. Yoshino, N. Mori, R. D. Rahimi, K. Sato, Y. Morita, K. Toyota, D. Shiomi, M. Kitagawa, H. Hara, P. Carl, P. Höfer, T. Takui, *Angew. Chem., Int. Ed.* **2012**, *51*, 9860.
[105] A. Fernandez, E. Moreno Pineda, C. A. Muryn, S. Sproules, F. Moro, G. A. Timco, E. J. L. McInnes, R. E. P. Winpenny, *Angew. Chem., Int. Ed.* **2015**, *54*, 10858.
[106] J. H. Olshansky, S. M. Harvey, M. L. Pennel, M. D. Krzyaniak, R. D. Schaller, M. R. Wasielewski, *J. Am. Chem. Soc.* **2020**, *142*, 13590.
[107] D. H. Waldeck, R. Naaman, Y. Paltiel, *APL Mater.* **2021**, *9*, 040902.
[108] S. Mishra, A. K. Mondal, S. Pal, T. K. Das, E. Z. B. Smolinsky, G. Siligardi, R. Naaman, *J. Phys. Chem. C* **2020**, *124*, 10776.
[109] The fact that the conductivity for the up magnetization is larger both for positive and negative voltages is due to the combined effect of CISS and opposite spins of the moving electrons at opposite voltages (in a setup with only one magnetic lead).
[110] C. Kulkarni, A. K. Mondal, T. K. Das, G. Grinbom, F. Tassinari, M. F. J. Mabesoone, E. W. Meijer, R. Naaman, *Adv. Mater.* **2020**, *32*, 1904965.
[111] H. Lu, J. Wang, C. Xiao, X. Pan, X. Chen, R. Brunecky, J. J. Berry, K. Zhu, M. C. Beard, Z. V. Vardeny, *Sci. Adv.* **2019**, *5*, eaay0571.
[112] Y. Lu, Q. Wang, R. He, F. Zhou, X. Yang, D. Wang, H. Cao, W. He, F. Pan, Z. Yang, C. Song, *Angew. Chem., Int. Ed.* **2021**, *60*, 23578.
[113] U. Huizi-Rayo, J. Gutierrez, J. M. Seco, V. Mujica, I. Diez-Perez, J. M. Ugalde, A. Tercjak, J. Cepeda, E. San Sebastian, *Nano Lett.* **2020**, *20*, 8476.
[114] R. Rodríguez, C. Naranjo, A. Kumar, P. Matozzo, T. K. Das, Q. Zhu, N. Vanthuyne, R. Gómez, R. Naaman, L. Sánchez, J. Crassous, *J. Am. Chem. Soc.* **2022**, *144*, 7709.
[115] T. N. H. Nguyen, L. Rasabathina, O. Hellwig, A. Sharma, G. Salvan, S. Yochelis, Y. Paltiel, L. T. Baczewski, C. Tegenkamp, *ACS Appl. Mater. Interfaces* **2022**, *14*, 38013.
[116] J. Gersten, K. Kaasbjerg, A. Nitzan, *J. Chem. Phys.* **2013**, *139*, 114111.
[117] M. Kettner, V. V. Maslyuk, D. Nürenberg, J. Seibel, R. Gutierrez, G. Cuniberti, K.-H. Ernst, H. Zacharias, *J. Phys. Chem. Lett.* **2018**, *9*, 2025.
[118] Y. Adhikari, T. Liu, H. Wang, Z. Hua, H. Liu, E. Lochner, P. Schlottmann, B. Yan, J. Zhao, P. Xiong, *arXiv:2209.08117*, **2022**.
[119] C. Fontanesi, E. Capua, Y. Paltiel, D. H. Waldeck, R. Naaman, *Adv. Mater.* **2018**, *30*, 1707390.
[120] It remains to understand which part of the electron transfer through photosystems I causes the observed spin selective transport.

Indeed, trEPR on the RP $P_{700}^{+\cdot}A_1^{-\cdot}$ in photosystem I at ambient as well as at low temperatures point to an initially populated singlet spin state.[94,121]

[121] S. Weber, T. Berthold, E. Ohmes, M. C. Thurnauer, J. R. Norris, G. Kothe, *Appl. Magn. Reson.* **1996**, *11*, 461.
[122] B. P. Bloom, B. M. Graff, S. Ghosh, D. N. Beratan, D. H. Waldeck, *J. Am. Chem. Soc.* **2017**, *139*, 9038.
[123] A. Kumar, E. Capua, M. K. Kesharwani, J. M. L. Martin, E. Sitbon, D. H. Waldeck, R. Naaman, *Proc. Natl. Acad. Sci. USA* **2017**, *114*, 2474.
[124] F. Tassinari, J. Steidel, S. Paltiel, C. Fontanesi, M. Lahav, Y. Paltiel, R. Naaman, *Chem. Sci.* **2019**, *10*, 5246.
[125] O. B. Dor, S. Yochelis, A. Radko, K. Vankayala, E. Capua, A. Capua, S.-H. Yang, L. T. Baczewski, S. S. P. Parkin, R. Naaman, Y. Paltiel, *Nat. Commun.* **2017**, *8*, 14567.
[126] T. K. Das, F. Tassinari, R. Naaman, J. Fransson, *J. Phys. Chem. C* **2022**, *126*, 3257.
[127] S. S. Chandran, Y. Wu, H.-H. Teh, D. H. Waldeck, J. E. Subotnik, *J. Chem. Phys.* **2022**, *156*, 174113.
[128] T. P. Fay, D. T. Limmer, *Nano Lett.* **2021**, *21*, 6696.
[129] L. M. K. Vandersypen, H. Bluhm, J. S. Clarke, A. S. Dzurak, R. Ishihara, A. Morello, D. J. Reilly, L. R. Schreiber, M. Veldhorst, *npj Quantum Inf.* **2017**, *3*, 34.
[130] The sequence is a simplified version (in quantum information terminology) of the three controlled-NOT operations yielding a SWAP gate between the states of A and Q. If we are not interested in the final state of A, we can reduce the sequence to only two pulses, even in case of incomplete polarization (due to limited CISS efficiency) and for any initial state of Q.
[131] A. S. Lukas, P. J. Bushard, M. R. Wasielewski, *J. Am. Chem. Soc.* **2001**, *123*, 2440.
[132] A. Farazdel, M. Dupuis, E. Clementi, A. Aviram, *J. Am. Chem. Soc.* **1990**, *112*, 4206.
[133] P. Li, P. Song, Q. Zhou, C. Du, Y. Ding, L. Xia, *J. Lumin.* **2016**, *177*, 325.
[134] H. J. Lee, T. Shimizu, H. Funakubo, Y. Imai, O. Sakata, S. H. Hwang, T. Y. Kim, C. Yoon, C. Dai, L. Q. Chen, S. Y. Lee, J. Y. Jo, *Phys. Rev. Lett.* **2019**, *123*, 217601.
[135] T. Heeren, J. Camp, J. Kolb, K. Schoenbach, S. Katsuki, H. Akiyama, *IEEE Trans. Dielectr. Electr. Insul.* **2007**, *14*, 884.
[136] A. R. Ruiz-Fernández, L. Campos, S. E. Gutierrez-Maldonado, G. Núñez, F. Villanelo, T. Perez-Acle, *Int. J. Mol. Sci.* **2022**, *23*, 11.
[137] A. Chatterjee, P. Stevenson, S. De Franceschi, A. Morello, N. P. de Leon, F. Kuemmeth, *Nat. Rev. Phys.* **2021**, *3*, 157.
[138] L. P. Kouwenhoven, C. M. Marcus, P. L. McEuen, S. Tarucha, R. M. Westervelt, N. S. Wingreen, in *Electron Transport in Quantum Dots*, Springer, Dordrecht, The Netherlands **1997**, pp. 105–214.
[139] M. R. Hummon, A. J. Stollenwerk, V. Narayanamurti, P. O. Anikeeva, M. J. Panzer, V. Wood, V. Bulović, *Phys. Rev. B* **2010**, *81*, 115439.
[140] J. M. Elzerman, R. Hanson, L. H. Willems van Beveren, B. Witkamp, L. M. K. Vandersypen, L. P. Kouwenhoven, *Nature* **2004**, *430*, 431.
[141] J. R. Petta, A. C. Johnson, J. M. Taylor, E. A. Laird, A. Yacoby, M. D. Lukin, C. M. Marcus, M. P. Hanson, A. C. Gossard, *Science* **2005**, *309*, 2180.
[142] C. H. Yang, W. H. Lim, F. A. Zwanenburg, A. S. Dzurak, *AIP Adv.* **2011**, *1*, 042111.
[143] A. Morello, J. J. Pla, F. A. Zwanenburg, K. W. Chan, K. Y. Tan, H. Huebl, M. Möttönen, C. D. Nugroho, C. Yang, J. A. van Donkelaar, A. D. C. Alves, D. N. Jamieson, C. C. Escott, L. C. L. Hollenberg, R. G. Clark, A. S. Dzurak, *Nature* **2010**, *467*, 687.
[144] C. H. Yang, R. C. C. Leon, J. C. C. Hwang, A. Saraiva, T. Tanttu, W. Huang, J. Camirand Lemyre, K. W. Chan, K. Y. Tan, F. E. Hudson, K. M. Itoh, A. Morello, M. Pioro-Ladrière, A. Laucht, A. S. Dzurak, Nature *580*, 350.
[145] F. Elste, C. Timm, *Phys. Rev. B* **2005**, *71*, 155403.
[146] A. Chiesa, E. Macaluso, P. Santini, S. Carretta, E. Pavarini, *Phys. Rev. B* **2019**, *99*, 235145.
[147] D. L. Klein, P. L. McEuen, J. E. B. Katari, R. Roth, A. P. Alivisatos, *Appl. Phys. Lett.* **1996**, *68*, 2574.
[148] M. Alves-Santos, R. D. Felice, G. Goldoni, *J. Phys. Chem. C* **2010**, *114*, 3776.
[149] D. V. Redžic, *Am. J. Phys.* **1994**, *62*, 1118.
[150] J. A. Stratton, *Electromagnetic Theory*, McGraw-Hill, New York **1941**.
[151] *Introducing Molecular Electronics*, Vol. *680*, (Eds: G. Cuniberti, K. Richter, G. Fagas), Springer, Berlin, Heidelberg **2006**.
[152] The two qubits can be made distinguishable by using slightly different g_i, which does not prevent implementation of the *i*SWAP$^{\alpha}$ gate, for instance by using a longitudinal magnetic field drive.[153]
[153] S. J. Lockyer, A. Chiesa, G. A. Timco, E. J. L. McInnes, T. S. Bennett, I. J. Vitorica-Yrezebal, S. Carretta, R. E. P. Winpenny, *Chem. Sci.* **2021**, *12*, 9104.
[154] M. Natali, S. Campagna, F. Scandola, *Chem. Soc. Rev.* **2014**, *43*, 4005.
[155] A. L. Efros, M. Rosen, M. Kuno, M. Nirmal, D. J. Norris, M. Bawendi, *Phys. Rev. B* **1996**, *54*, 4843.
[156] A. K. Mondal, M. D. Preuss, M. L. Sleczkowski, T. K. Das, G. Vantomme, E. W. Meijer, R. Naaman, *J. Am. Chem. Soc.* **2021**, *143*, 7189.
[157] A. Privitera, D. Faccio, D. Giuri, D. Genovese, F. Tassinari, L. Mummolo, M. Chiesa, C. Fontanesi, E. Salvadori, A. Cornia, C. Tomasini, R. Sessoli, *ChemRxiv* **2020**, https://doi.org/10.26434/chemrxiv–2022–dx58w
[158] L. Garbuio, S. Antonello, I. Guryanov, Y. Li, M. Ruzzi, N. J. Turro, F. Maran, *J. Am. Chem. Soc.* **2012**, *134*, 10628.
[159] T. Morita, S. Kimura, *J. Am. Chem. Soc.* **2003**, *125*, 8732.
[160] Y. Arikuma, H. Nakayama, T. Morita, S. Kimura, *Langmuir* **2011**, *27*, 1530.
[161] R. Naaman, D. H. Waldeck, J. Fransson, *J. Phys. Chem. Lett.* **2022**, *13*, 11753.
[162] M. R. Wasielewski, M. P. Niemczyk, D. G. Johnson, W. A. Svec, D. W. Minsek, *Tetrahedron* **1989**, *45*, 4785.
[163] T. Mani, *Chem. Phys. Rev.* **2022**, *3*, 021301.
[164] P. K. Poddutoori, N. Zarrabi, A. G. Moiseev, R. Gumbau-Brisa, S. Vassiliev, A. van der Est, *Chem. Eur. J.* **2013**, *19*, 3148.
[165] M. Di Valentin, A. Bisol, G. Agostini, P. A. Liddell, G. Kodis, A. L. Moore, T. A. Moore, D. Gust, D. Carbonera, *J. Phys. Chem. B* **2005**, *109*, 14401.
[166] M. Gingras, G. Félix, R. Peresutti, *Chem. Soc. Rev.* **2013**, *42*, 1007.
[167] V. Kiran, S. P. Mathew, S. R. Cohen, I. Hernández Delgado, J. Lacour, R. Naaman, *Adv. Mater.* **2016**, *28*, 1957.
[168] Y. Liang, K. Banjac, K. Martin, N. Zigon, S. Lee, N. Vanthuyne, F. A. Garcés-Pineda, J. R. Galán-Mascarós, X. Hu, N. Avarvari, M. Lingenfelder, *Nat. Commun.* **2022**, *13*, 3356.
[169] W. Mtangi, V. Kiran, C. Fontanesi, R. Naaman, *J. Phys. Chem. Lett.* **2015**, *6*, 4916.
[170] K. Dhbaibi, L. Abella, S. Meunier-Della-Gatta, T. Roisnel, N. Vanthuyne, B. Jamoussi, G. Pieters, B. Racine, E. Quesnel, J. Autschbach, J. Crassous, L. Favereau, *Chem. Sci.* **2021**, *12*, 5522.
[171] Y.-Z. Dai, B.-W. Dong, Y. Kao, Z.-Y. Wang, H.-I. Un, Z. Liu, Z.-J. Lin, L. Li, F.-B. Xie, Y. Lu, M.-X. Xu, T. Lei, Y.-J. Sun, J.-Y. Wang, S. Gao, S.-D. Jiang, J. Pei, *ChemPhysChem* **2018**, *19*, 2972.
[172] F. Lombardi, A. Lodi, J. Ma, J. Liu, M. Slota, A. Narita, W. K. Myers, K. Müllen, X. Feng, L. Bogani, *Science* **2019**, *366*, 1107.
[173] A. M. Ariciu, D. H. Woen, D. N. Huh, L. E. Nodaraki, A. K. Kostopoulos, C. A. P. Goodwin, N. F. Chilton, E. J. L. McInnes, R. E. P. Winpenny, W. J. Evans, F. Tuna, *Nat. Commun.* **2019**, *10*, 3330.
[174] T. Liu, X. Wang, H. Wang, G. Shi, F. Gao, H. Feng, H. Deng, L. Hu, E. Lochner, P. Schlottmann, S. von Molnár, Y. Li, J. Zhao, P. Xiong, *ACS Nano* **2020**, *14*, 15983.
[175] A. Lunghi, S. Sanvito, *Sci. Adv.* **2019**, *5*, eaax7163.

[176] A. Albino, S. Benci, M. Atzori, L. Chelazzi, S. Ciattini, A. Taschin, P. Bartolini, A. Lunghi, R. Righini, R. Torre, F. Totti, R. Sessoli, *J. Phys. Chem. C* **2021**, *125*, 22100.
[177] A. Lunghi, *Sci. Adv.* **2022**, *8*, eabn7880.
[178] M. J. Amdur, K. R. Mullin, M. J. Waters, D. Puggioni, M. K. Wojnar, M. Gu, L. Sun, P. H. Oyala, J. M. Rondinelli, D. E. Freedman, *Chem. Sci.* **2022**, *13*, 7034.
[179] E. Garlatti, A. Albino, S. Chicco, V. Nguyen, F. Santanni, L. Paolasini, C. Mazzoli, R. Caciuffo, F. Totti, P. Santini, R. Sessoli, A. Lunghi, S. Carretta, *Nat. Commun.* **2023**.
[180] C. F. Koelsch, *J. Am. Chem. Soc.* **1957**, *79*, 4439.
[181] Y. H. Huang, M. D. Krzyaniak, R. M. Young, M. R. Wasielewski, *Appl. Magn. Reson.* **2022**, *53*, 949.
[182] H. Mao, R. M. Young, M. D. Krzyaniak, M. R. Wasielewski, *J. Phys. Chem. B* **2022**, *126*, 10519.
[183] S. Nakazawa, S. Nishida, T. Ise, T. Yoshino, N. Mori, R. D. Rahimi, K. Sato, Y. Morita, K. Toyota, D. Shiomi, M. Kitagawa, H. Hara, P. Carl, P. Häfer, T. Takui, *Angew. Chem., Int. Ed.* **2012**, *51*, 9860.
[184] S. von Kugelgen, M. D. Krzyaniak, M. Q. Gu, D. Puggioni, J. M. Rondinelli, M. R. Wasielewski, D. E. Freedman, *J. Am. Chem. Soc.* **2021**, *143*, 8069.
[185] E. R. Canarie, S. M. Jahn, S. Stoll, *J. Phys. Chem. Lett.* **2020**, *11*, 3396.
[186] M. J. Graham, C. J. Yu, M. D. Krzyaniak, M. R. Wasielewski, D. E. Freedman, *J. Am. Chem. Soc.* **2017**, *139*, 3196.
[187] C. Godfrin, A. Ferhat, R. Ballou, S. Klyatskaya, M. Ruben, W. Wernsdorfer, F. Balestro, *Phys. Rev. Lett.* **2017**, *119*, 187702.
[188] M. Atzori, E. Garlatti, G. Allodi, S. Chicco, A. Chiesa, A. Albino, R. D. Renzi, E. Salvadori, M. Chiesa, S. Carretta, L. Sorace, *Inorg. Chem.* **2021**, *60*, 11273.
[189] T. Yamabayashi, M. Atzori, L. Tesi, G. Cosquer, F. Santanni, M.-E. Boulon, E. Morra, S. Benci, R. Torre, M. Chiesa, L. Sorace, R. Sessoli, M. Yamashita, *J. Am. Chem. Soc.* **2018**, *140*, 12090.
[190] J. M. Van Raden, D. I. Alexandropoulos, M. Slota, S. Sopp, T. Matsuno, A. L. Thompson, H. Isobe, H. L. Anderson, L. Bogani, *J. Am. Chem. Soc.* **2022**, *144*, 8693.
[191] K. Likharev, *Proc. IEEE* **1999**, *87*, 606.
[192] J. Jalil, Y. Zhu, C. Ekanayake, Y. Ruan, *Nanotechnology* **2017**, *28*, 142002.
[193] F. J. Schupp, *J. Mater. Sci. Technol.* **2017**, *33*, 944.
[194] S. J. Shin, C. S. Jung, B. J. Park, T. K. Yoon, J. J. Lee, S. J. Kim, J. B. Choi, Y. Takahashi, D. G. Hasko, *Appl. Phys. Lett.* **2010**, *97*, 103101.
[195] S. J. Shin, J. J. Lee, H. J. Kang, J. B. Choi, S.-R. E. Yang, Y. Takahashi, D. G. Hasko, *Nano Lett.* **2011**, *11*, 1591.
[196] A. S. Katkar, S. P. Gupta, C. Granata, C. Nappi, W. Prellier, L.-J. Chen, P. S. Walke, *ACS Appl. Electron. Mater.* **2020**, *2*, 1843.
[197] N. P. de Leon, K. M. Itoh, D. Kim, K. K. Mehta, T. E. Northup, H. Paik, B. S. Palmer, N. Samarth, S. Sangtawesin, D. W. Steuerman, *Science* **2021**, *372*, eabb2823.
[198] S. Willing, H. Lehmann, M. Volkmann, C. Klinke, *Sci. Adv.* **2017**, *3*, e1603191.
[199] R. P. Andres, T. Bein, M. Dorogi, S. Feng, J. I. Henderson, C. P. Kubiak, W. Mahoney, R. G. Osifchin, R. Reifenberger, *Science* **1996**, *272*, 1323.
[200] H. Park, J. Park, A. K. L. Lim, E. H. Anderson, A. P. Alivisatos, P. L. McEuen, *Nature* **2000**, *407*, 57.
[201] L. Torsi, M. Magliulo, K. Manoli, G. Palazzo, *Chem. Soc. Rev.* **2013**, *42*, 8612.
[202] Y. Guo, C.-A. Di, S. Ye, X. Sun, J. Zheng, Y. Wen, W. Wu, G. Yu, Y. Liu, *Adv. Mater.* **2009**, *21*, 1954.
[203] L. A. Frolova, P. A. Troshin, D. K. Susarova, A. V. Kulikov, N. A. Sanina, S. M. Aldoshin, *Chem. Commun.* **2015**, *51*, 6130.
[204] Y. J. Jeong, D.-J. Yun, S. H. Kim, J. Jang, C. E. Park, *ACS Appl. Mater. Interfaces* **2017**, *9*, 11759.
[205] L. A. Frolova, Y. Furmansky, A. F. Shestakov, N. A. Emelianov, P. A. Liddell, D. Gust, I. Visoly-Fisher, P. A. Troshin, *ACS Appl. Mater. Interfaces* **2022**, *14*, 15461.
[206] D. Kaplan, I. Solomon, N. F. Mott, *J. Phys. Lett.* **1978**, *39*, 51.
[207] A. Honig, *Phys. Rev. Lett.* **1966**, *17*, 186.
[208] R. Maxwell, A. Honig, *Phys. Rev. Lett.* **1966**, *17*, 188.
[209] D. J. Lepine, *Phys. Rev. B* **1972**, *6*, 436.
[210] L. A. Ladd, W. Paul, *Solid State Commun.* **1969**, *7*, 425.
[211] C. Boehme, K. Lips, *Phys. Rev. Lett.* **2003**, *91*, 246603.
[212] P. C. Y. Chow, N. Matsuhisa, P. Zalar, M. Koizumi, T. Yokota, T. Someya, *Nat. Commun.* **2018**, *9*, 4546.
[213] M. Nikolka, D. Simatos, A. Foudeh, R. Pfattner, I. McCulloch, Z. Bao, *ACS Appl. Mater. Interfaces* **2020**, *12*, 40581.